TAMPEREEN TEKNILLINEN YLIOPISTO
TAMPERE UNIVERSITY OF TECHNOLOGY

**MARIA RAIKO**

# EVALUATION OF A NOVEL CRYOGENIC OXYGEN ENRICHMENT METHOD

Master's thesis

Examiner: Adjunct Professor Hannu Ahlstedt
Examiner and topic approved by the Council of the Faculty of Natural Sciences on 7 October 2015

# ABSTRACT

**MARIA RAIKO**: Evaluation of a Novel Cryogenic Oxygen Enrichment Method
Tampere University of Technology
Master of Science Thesis, 61 pages
January 2016
Master's Degree Programme in Environmental and Energy Engineering
Major: Power Plant and Combustion Technology
Examiner: Adjunct Professor Hannu Ahlstedt

Keywords: Oxygen enrichment, Air separation, Process simulation

The goal of this thesis was to study and evaluate the Nurmia oxygen enrichment process and to compare it with the conventional Linde-Frankl oxygen separation method. The study includes studying both processes, creating a simulation model of the Nurmia oxygen enrichment process, carrying out simulations with different oxygen product purities and the analysis of the simulation results with a comparison to literature values.

The simulation model was assembled according to a basic apparatus of the Nurmia oxygen enrichment process. A sensitivity analysis was performed to verify the functionality of the model. In the simulation results the product purity per compressor power is higher than what is presented in literature, which is caused by partial idealizations in the subprocesses of the simulation model. Otherwise the simulation results corresponded well to the process values presented in literature.

The Nurmia oxygen enrichment process is found to enable oxygen concentrate production with better efficiency than the conventional oxygen separation process Linde-Frankl. The power consumption of compression for Nurmia process varies from 75 to 111 kWh/ton of oxygen product depending on the chosen process configuration. Lowering the purity decreases the energy consumption. For the conventional Linde-Frankl process the power consumption from compression work is approximately 245 kWh/ton of oxygen product. The flexibility of the Nurmia process is also better because the Nurmia oxygen enrichment method allows producing oxygen product with purity from 50 mol-% to 99 mol-% depending on the process configuration. For Linde-Frankl process the oxygen content of product is 99.5 mol-% or more.

A dynamic simulation model is recommended to be carried out next to investigate the functionality of the process start-up and process control. Also construction of a demo-scale plant is recommended to verify the simulation results.

# TIIVISTELMÄ

**MARIA RAIKO**: Uuden kryogeenisen hapenrikastusmenetelmän arviointi
Tampereen teknillinen yliopisto
Diplomityö, 61 sivua
Tammikuu 2016
Ympäristö- ja energiatekniikan diplomi-insinöörin tutkinto-ohjelma
Pääaine: Voimalaitos- ja polttotekniikka
Tarkastaja: dosentti Hannu Ahlstedt

Avainsanat: Hapen rikastaminen, ilmatislaus, prosessisimulointi

Työn tavoitteena oli tutkia ja arvioida Matti Nurmian kehittämää hapenrikastusprosessia ja verrata sitä yleisesti käytettyyn Linde-Frankl -ilmatislausmenetelmään. Työssä tarkasteltiin molempia prosesseja, luotiin simulointimalli Nurmian hapenrikastusprosessista, suoritettiin simulaatioita eri vahvuisia happituotteita tuottaen ja analysoitiin simuloinnin tulokset kirjallisuudessa esitettyihin prosessiarvoihin vertaillen.

Simulointimalli tehtiin Nurmian hapenrikastusprosessin peruslaitteiston mukaiseksi. Simulointimallille suoritettiin herkkyysanalyysi, jolla mallin toimivuus varmistettiin. Simuloinnin tuloksina saatu happituotteen puhtauden arvo kompressoritehoon nähden on hieman kirjallisuusarvoa korkeampi, mikä johtuu simulointimallin osaprosessien osittaisista idealisoinneista. Muilta osin simuloinnin tulokset vastasivat hyvin kirjallisuudessa esitettyjä arvoja.

Nurmian hapenrikastusprosessin havaittiin pystyvän tuottamaan happituotetta paremmalla hyötysuhteella kuin Linde-Frankl -prosessi. Nurmian hapenrikastusprosessissa kompressorityön aiheuttama energiantarve vaihtelee happituotetonnia kohden 75–111 kWh/t välillä, riippuen prosessin kokoonpanosta. Tuotteen happipitoisuuden laskeminen vähentää prosessin energiankulutusta. Linde-Frankl –prosessin vaatima kompressorityö tuotettua happitonnia kohden on noin 245 kWh/t. Nurmian prosessi on myös joustavampi lopputuotteen happipitoisuuden suhteen, koska sillä pystytään tuottamaan happituotetta 50 mol-%:n happipitoisuudesta 99 mol-%:iin asti, prosessin säädöistä riippuen. Linde-Frankl -prosessin tuottama happipitoisuus on yli 99,5 mol-%.

Seuraavaksi olisi suositeltavaa toteuttaa dynaaminen simulointimalli, jotta prosessin toimintaa voitaisiin tarkastella myös prosessin käynnistys- ja ohjaustilanteissa. Myös demonstraatiolaitoksen rakentaminen on tärkeää simuloinnin tulosten vahvistamisen kannalta.

# PREFACE

This work was carried out at the Tampere University of Technology on the department of Chemistry and Bioengineering, starting in March 2015 and finished in December 2015.

I would like to thank Hannu Ahlstedt for providing me the opportunity to work on this thesis and Matti Nurmia for his valuable advice regarding this work. I would also like to express my gratitude towards my family and friends for their support during this work.

Tampere, December 2015

Maria Raiko

# CONTENTS

# TERMS AND DEFINITIONS

| | |
|---|---|
| Air distillation | The process separating different components of by means of distillation |
| Air rectification | The process separating different components of air by means of rectification |
| Air separation | The process of separating different components of air |
| ASU | Air Separation Unit |
| CCS | Carbon Capture and Storage |
| Double column | Two interconnected separation columns |
| Joule-Thomson effect | The change in temperature that occurs when a non-ideal gas or fluid is adiabatically throttled at constant enthalpy |
| Linde-Frankl process | Air separation process using double column and regenerative heat exchanger |
| Linde liquefaction cycle | Air liquefaction process based on Joule-Thomson effect |
| Nested column | Two interconnected separation columns one of which is located nested inside the other |
| Nitrogen concentrate | Air with increased nitrogen fraction |
| Nurmia oxygen enrichment process | Air separation process using nested double column and low pressure level |
| Oxyfuel combustion | Carbon capture method based on the use of pure oxygen diluted with recycled flue gas for combustion instead of air |
| Oxygen concentrate | Air with increased oxygen fraction |
| Separation column | A distillation or rectification column used in air separation process |

# NOMENCLATURE

| | |
|---|---|
| a | Peng-Robinson equation constant [(kg $m^5$) / ($mol^2$ $s^2$)] |
| A | area [$m^2$] |
| b | Peng-Robinson equation constant [$m^3$/mol] |
| c | molar concentration [mol/$m^3$] |
| $c_p$ | specific heat at constant pressure [J/(kg K)] |
| $c_v$ | specific heat at constant volume [J/(kg K)] |
| D | diffusion coefficient [$m^2$/s] |
| g | gravitational acceleration [m/$s^2$] |
| H | molar enthalpy [J/mol] |
| h | heat transfer coefficient [W/($m^2$ K)], enthalpy [J/kg] |
| $h_{fg}$ | latent heat of condensation [J/mol], [J/kg] |
| Ja | Jakob number |
| k | thermal conductivity [W/(m K)] |
| $k_m$ | mass transfer coefficient [m/s] |
| L | length [m] |
| M | molar mass [kg/kmol] |
| m | mass [kg] |
| $\dot{m}$ | mass flow [kg/s] |
| $\dot{m}''$ | mass flux [kg/($m^2$ s)] |
| $\dot{N}''$ | molar flux [kmol/($m^2$ s)] |
| p | pressure [Pa] |
| Pr | Prandtl number |
| Q | thermal energy [J] |
| $\dot{Q}$ | thermal flow [W] |

| | |
|---|---|
| $\dot{Q}''$ | thermal flow per area [W/m$^2$] |
| P | mechanical power [W], perimeter [m] |
| R | universal gas constant [J/(mol K)] |
| $R_i$ | gas constant for gas i [J/(kg K)] |
| Re | Reynolds number |
| T | temperature [K] |
| $T_r$ | reduced temperature [-] |
| U | velocity [m/s] |
| V | volume [m$^3$] |
| $V_m$ | molar volume [m$^3$/mol] |
| v | specific volume [m$^3$/kg] |
| W | mechanical work [J] |
| x | molar fraction [-], position parallel to height [m] |
| $\alpha$ | Peng-Robinson equation coefficient [-] |
| $\beta$ | thermal expansion coefficient [1/K] |
| $\Gamma$ | flow rate per unit width [kg/(m s)] |
| $\gamma$ | isentropic constant [-] |
| $\delta$ | film thickness [m], boundary layer thickness [m] |
| $\varepsilon$ | heat exchanger effectiveness [-] |
| $\eta_s$ | isentropic efficiency [-] |
| $\kappa$ | Peng-Robinson equation coefficient [-] |
| $\mu_l$ | dynamic viscosity [kg/(m s)] |
| $\nu_i$ | kinematic viscosity [m$^2$/s], |
| $\rho$ | density [kg/m$^3$] |
| $\omega$ | acentric factor [-] |

# 1. INTRODUCTION

Cryogenic oxygen separation is currently the dominant technology for large scale air separation units used in industrial applications, such as oxyfuel combustion, oxygen-enhanced combustion and steel industry. Other oxygen separation technologies include ceramic and polymeric membranes, pressure swing adsorption and vacuum swing adsorption, but they are not economically feasible in a large enough scale. (Teir et al. 2011, Tranier et al. 2011)

Nurmia oxygen enrichment method is a novel cryogenic process that enables economical manufacture of oxygen enriched air (Nurmia 2003). The objective of this thesis is to investigate the Nurmia oxygen enrichment process by means of a simulation model and compare it with the conventional Linde-Frankl oxygen separation process. Also a comparison of their feasibility for different industrial applications is carried out. The simulation model is assembled using Aspen Plus. The sizing of process devices, such as heat exchangers and compressors, is carried out using the simulation model, while also taking the internal heat transfer in the process into account. The patent of Nurmia oxygen enrichment process presents several different process options of which one in chosen to be simulated. Two simulations are carried out with different oxygen contents of the process product.

The functionality of the Nurmia oxygen enrichment process in practice has been previously verified by studies at the Tampere University of Technology and thus the functionality of the process does not need to be demonstrated in this thesis (Saarenpää 2002; Saarenpää et al. 2004).

The air separation processes are discussed in Chapter 2, including process descriptions of both Linde-Frankl and Nurmia oxygen enrichment process. Some physical properties of air and its components in cryogenic conditions are listed in Chapter 3 to illustrate the conditions where the processes operate. The subprocesses of Nurmia oxygen enrichment process are described in Chapter 4. In Chapter 5 there is a presentation of the simulation model, the results of the simulations and a sensitivity analysis to verify the functionality of the model. The results and a comparison between the air separation methods Nurmia and Linde-Frankl are discussed in Chapter 6. Finally, the conclusions of the thesis are presented in Chapter 7.

# 2. AIR SEPARATION

The first technique to separate the components of air was invented over a century ago. It was based on the distillation of liquefied air. Today there are several process options available, but the most common methods are still based on air liquefaction and distillation. (Agrawal & Herron 2000, p. 1895; Mersmann et al. 2011, p. 601)

## 2.1 Large scale oxygen production for industrial applications

Industrial applications such as oxyfuel combustion, oxygen-enhanced combustion and steel industry require large volumes of either pure oxygen or enriched oxygen concentrate. Large scale processes have an air separation unit to provide the oxygen needed. For example in oxyfuel combustion the air separation unit needs to be able to deliver large volumes of oxygen, typically over 8000 t/d, at a low pressure, moderate purity of 85-98 mol-% and maximal energy efficiency. (Darde et al. 2009; Tranier et al. 2011, p. 968; 3rd Oxyfuel Combustion Conference Summary 2013)

Air separation can be performed by using cryogenic separation, which is currently the only commercially available method to economically produce large enough volumes of oxygen to be used in oxyfuel combustion power plant or other major oxygen-intensive industrial applications (Teir et al. 2011; Tranier et al. 2011). Other possible oxygen separation methods include ceramic and polymeric membranes, pressure swing adsorption and vacuum swing adsorption (Tranier et al. 2011).

Oxyfuel combustion is a carbon capture method based on the use of pure oxygen diluted with recycled flue gas for combustion instead of air. The oxygen is diluted with flue gas in order to control the combustion temperature. The extraction of $CO_2$ is easier for oxyfuel combustion process than in conventional combustion process due to its higher concentration in flue gas and smaller flue gas overall volume. This follows from the fact that it does not contain nitrogen from the combustion air. (Teir et al. 2011)

Oxyfuel combustion systems consist of an air separation unit, the power plant and a $CO_2$ processing unit. Figure 1 illustrates an oxyfuel combustion system with integrated air separation unit and $CO_2$ treatment unit. A steam boiler operates by burning fuel with oxygen produced in the air separation unit. The steam is used to run a turbine to produce electricity and after this it is condensed and led back to the boiler. Flue gas from the burning of fuel consisting mainly of $CO_2$ is first filtered to remove fly ash and cooled to remove water vapor. Sulphur compounds are removed in a desulphurization process and

any remaining water is again removed by cooling. Finally, the $CO_2$ is compressed to allow easier transport and storage. (Teir et al. 2011)

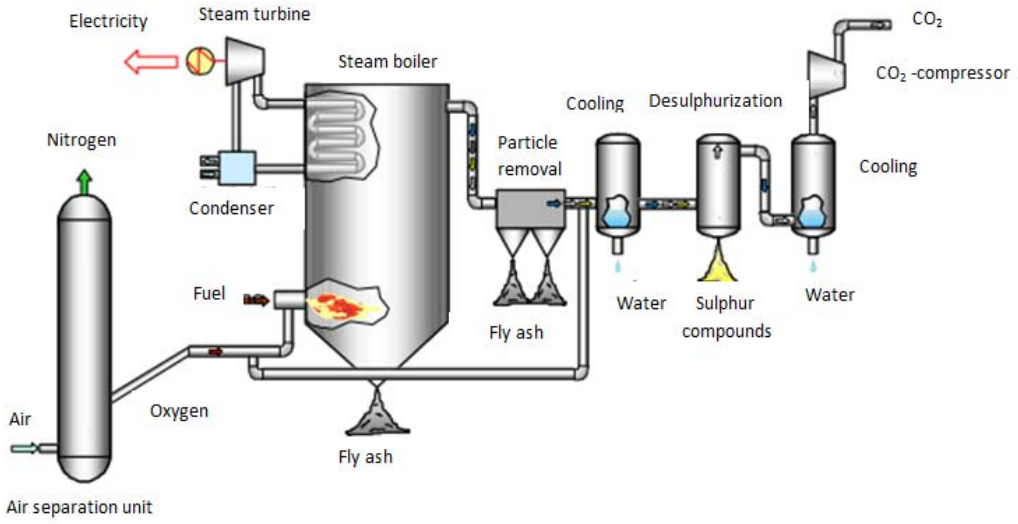


***Figure 1.*** *Carbon capture system using oxyfuel combustion and an air separation unit. (adapted from Teir et al. 2011)*

An air separation unit based on cryogenic separation consists of an air compressor, precooling equipment, a purification unit to filter and remove $H_2O$ and $CO_2$, heat exchangers, distillation columns, vaporizers and condensers. (Darde et al. 2009)

## 2.2 Cryogenic oxygen separation methods

The technology to separate the major components of air by distillation has been around for over a century. An important requirement to the said process is to achieve the very low temperature level needed to operate the distillation column. Thus air separation differs from typical distillation process, because it is not possible to cool the cryogenic columns with water or heat them with steam such as in common distillation processes. A refrigeration process is needed to achieve the low temperature level needed. (Agrawal & Herron 2000, p. 1895; Timmerhaus & Reed 2007, p. 6-9; Mersmann et al. 2011, p. 601)

Cryogenic air separation is now considered a mature technology. However, the energy efficiency of the process has developed over the last 30 years. Air separation processes manufacturing oxygen product with a lower purity were developed in the 1990s to inexpensively produce oxygen for the needs of oxygen enriching combustion air of furnaces and gasification; they have a separation energy of 200 kWh/t. Further optimization of the process is expected to reach a separation energy of approximately 140 kWh/t, if heat integration is used. (Tranier et al. 2011, p. 968)

In general, cryogenic oxygen separation methods are based on the liquefaction process of air and a multiple distillation process called rectification. Air rectification is possible because the boiling points of the components of air differ from each other. (Castle 2002; Mersmann et al. 2011, p. 251)

Saturation pressures of nitrogen and oxygen as a function of temperature are plotted in Figure 2, where normal boiling points in 1 bar are marked with arrows for both compounds. The boiling point for oxygen in 1 bar is 90.1878 K and for nitrogen 77.355 K. The plot is created using the Antoine equation from NIST WebBook database by Lemmon et al. and parameter data from Brower and Thodos. The saturation pressure is

$$\log_{10}(p) = A - \left(\frac{B}{T+C}\right) \qquad (2.1)$$

where $p$ is vapor pressure (bar) and $T$ is temperature (K). The parameter $A$ is 3.85845, $B$ is 325.675 and $C$ is -5.667. (Brower & Thodos 1968; Lemmon et al. 2015)

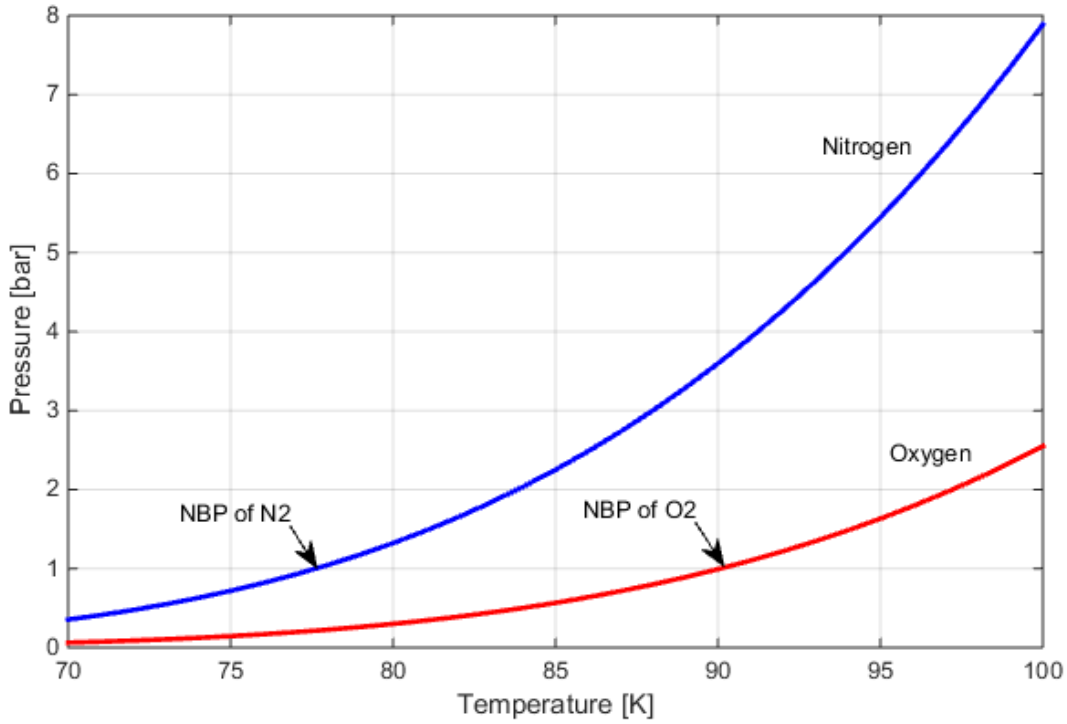


***Figure 2.*** *Saturation pressure curves of nitrogen and oxygen with their normal boiling points (in 1 atm) marked with black arrows.*

The different components of air are separated by means of their differing boiling points in a cascaded distillation process called air rectification. Air rectification consists of several consecutive condensation-vaporization cycles, also called theoretical plates, occurring in a fractionating rectification column or a configuration consisting of several interconnected columns. Repeated condensation and vaporization are able to produce

practically total separation of the components in most fluids. (Smith & Jobson 2000, p. 84-85; Mersmann et al. 2011, p. 251)

A distillation process has many advantages in comparison to other separation methods. These include the capability to handle a wide variety of flow rates, the capability to use feeds with highly varying concentrations and the capability to produce fractions with a very high purity. (Smith & Jobson 2000, p. 84)

In a rectification column the liquid air streams through a set of rectification plates. The liquid streams countercurrent to the gas rising up and absorbs less volatile oxygen from the gas while releasing more volatile nitrogen. Thus the liquid stream enriches with oxygen and the gas enriches with nitrogen. The gaseous nitrogen concentrate leaves the process from the top of the column as a waste stream. The oxygen enriched product is gathered from the lower part of the column either in a gaseous form or in liquid state. Usually, a very small amount of liquid oxygen product is always streamed from the bottom of the column in order to avoid build-up of impurities, such as hydrocarbons, in the column. (Agrawal & Herron 2000, p. 1897)

At air rectification processes, a section where the liquid and gas phases are in equilibrium is called a theoretical plate. A basic method for determining the number of theoretical plates in an air separation system involving two components is the McCabe-Thiele method, which is illustrated in Figure 3. The equilibrium curve in Figure 3 is plotted using data of composition in the function of temperature at the column pressure. Other operating lines are the bottoms composition, feed composition and distillate composition. The equilibrium states are determined by drawing orthogonal steps between the equilibrium curve and the operating lines. (Timmerhaus & Reed 2007, p. 111-113)

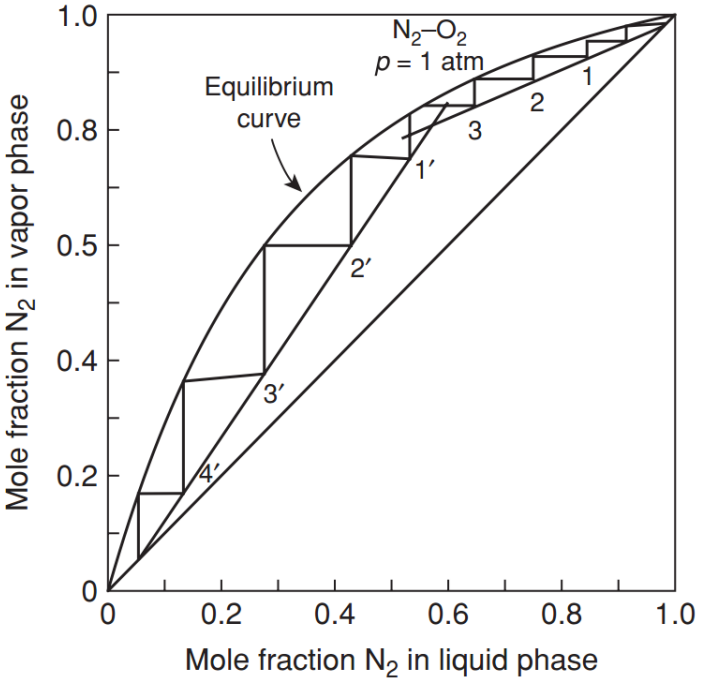


***Figure 3.*** *A McCabe-Thiele method-plot for theoretical liquid air distillation column working at 1 atm pressure. The theoretical plates are drawn as steps between the equilibrium curve and operating lines. The number of stages measures the difficulty of the separation. (Timmerhaus & Reed 2007 p. 112)*

The air needs to be pretreated before liquefaction in order to remove water and carbon dioxide, because these components would disturb the rectification process by solidifying at the temperatures used to liquefy air. The pre-treatment can be carried out for example by using molecular sieves or a refrigeration system (Castle 2002, p. 160). In some air separation methods, at least some of the water and carbon dioxide can be left in the process air, because they will freeze in the regenerative heat exchangers and exit along the counterflow (Agrawal & Herron 2000, p. 1908-1909).

The air liquifier differs from the conventional refrigeration process since it is an open system. In the liquifier process the liquid product is removed and therefore there must be a corresponding make-up stream into the process. The mass flow rate in different parts of the process is not constant because some of the liquid is removed. In refrigerators the mass flow is constant throughout the process and therefore a better countercurrent refrigerant effect can be achieved. (Flynn 2004, p. 359)

### 2.2.1 Linde-Frankl process

The Linde liquefaction cycle is a basic process to manufacture liquid air. In Linde-Frankl separation process, different kinds of process configurations exist, but the main characteristics are a double column consisting of high and low pressure sides and the regenerators used for heat exchange in the process. (Struchtrup 2014, p. 387)

The Linde liquefaction cycle is based on the Joule-Thomson effect of gases. The effect causes the temperature to drop significantly when the gas is rapidly expanded. A Joule-Thomson coefficient $(\partial T/\partial p)_h$ determines the change of temperature in an isenthalpic process. The inversion curve for real gases presented below describes whether the throttling process causes a temperature increase or a decrease

$$\left(\frac{\partial T}{\partial p}\right)_h = 0 \;\; or \;\; \beta = \frac{1}{T} \qquad (2.2)$$

where $T$ is temperature, $p$ is pressure, $h$ is enthalpy and $\beta$ is the coefficient of thermal expansion. For states below the inversion curve, pressure decrease leads to a decrease of temperature as well. (Linde engineering 2009; Struchtrup 2014, p. 387)

The Linde-Frankl separation process is based on fractional distillation and enrichment process. It consists of a high pressure column and a low pressure column connected from the upper end of the high pressure column to the lower end of the low pressure column. Thus a temperature difference between the top condenser and the lower part in each column is maintained. The temperature difference between the unconnected ends of the columns determines how close to reversibility does the process operate. (Nurmia 2003)

The Linde-Frankl process with two columns, as seen simplified in Figure 4, has a high pressure column and a low pressure column that are thermally connected. The pressure level of the high pressure column is typically approximately 6 bar and the pressure level of the low pressure column is usually a little over 1 bar. (Castle 2002, p. 161-163)

The input air is first pre-treated to remove impurities and compressed. The compressed air is then cooled in the heat exchanger until its dew point and injected to the high pressure column. A fraction of the air is further cooled down by an expansion turbine and/or a throttle in order to maintain the cold enough temperature in the process. The input air is separated in the column to an oxygen rich fraction that has an oxygen content of approximately 40 mol-%, and to a nitrogen rich gaseous fraction. The two product streams from the high pressure column are illustrated in Figure 4, one enriched with nitrogen (blue line in Figure 4) and the other enriched with oxygen (red line in Figure 4). The liquid oxygen enriched air is separated, throttled to the pressure level of the low pressure column and injected there. The nitrogen concentrate is also throttled and injected to the low pressure column. The vaporization of the liquid oxygen in the low pressure column causes the condensation of nitrogen in the high pressure column due to heat exchange between the two columns. If required, argon can be separated in an additional column. (Castle 2002, p. 161-163; Flynn 2004 p. 392-393; Mersmann et al. 2011, p. 601-602)

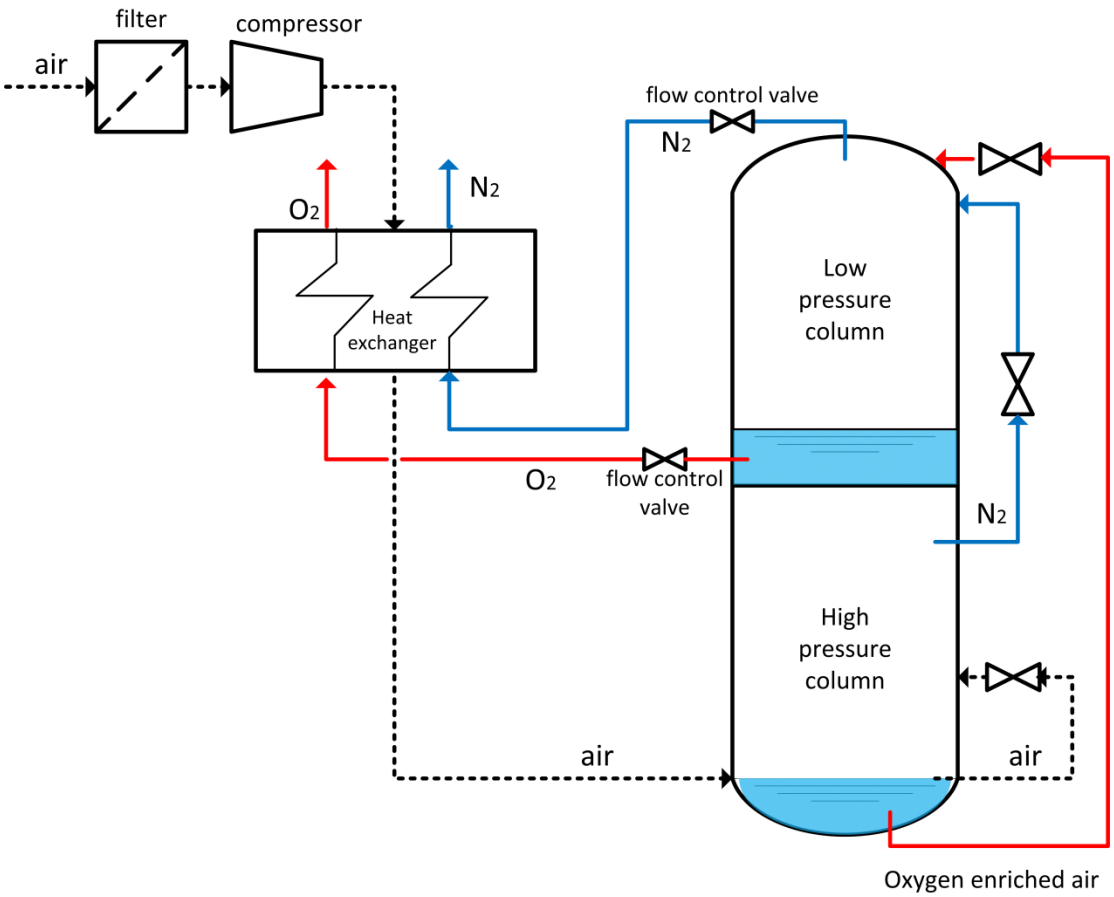


***Figure 4.*** *Simplified Linde-Frankl process model, where pretreated and compressed input air (marked with dashed line) is cooled down in a heat exchanger with the cold output flows. Then the air is led to high pressure column, where some of it is throttled to further cool it down. Liquid oxygen concentrate (red line) and gaseous nitrogen (blue line) produced in the high pressure column are first throttled to a lower pressure level and then led to low pressure column where finally nitrogen and oxygen are separated and led to the heat exchanger to cool down make-up air for the process. Flow control valves are at the exiting streams to prevent backflow.*

The heat exchanger type originally used in the Linde process was a large brazed aluminum plate and fin heat exchanger. In the 1930s, a regenerator was invented and adopted to the Linde-Frankl process, which enabled some moisture and carbon dioxide to be left in the process air, because the structure is self-cleaning. Currently the most popular heat exchanger type in air separation processes is recuperative counterflow plate and fin heat exchanger with adsorptive drying and cleaning upstream. (Agrawal & Herron 2000, p. 1908-1909)

The basic Linde liquefaction process, as presented in Figure 5, starts with a nearly isothermal compression of the process air to a higher than atmospheric pressure level (process stages 1-2). The nearly isothermal compression is carried out by cooling the air during the compression. After compression the air is treated in an oxidation chamber and water separator in order to remove $H_2O$ and $CO_2$ that would disturb the process. Then the air is streamed into a heat exchanger, which brings its temperature down to

almost the boiling point of air (process stages 2-3). The air then goes through isenthalpic throttling to the original pressure level, which causes a temperature drop and liquefaction (process stages 3-4). The liquid fraction (1-$x_4$) is led out of the process isothermally (process stages 4-P). Finally, the remaining fraction of air $x_4$ goes through the heat exchanger and receives heat from input air (process stages 5-6). (Chenier 2002, p. 41-43; Struchtrup 2014, p. 278-279)

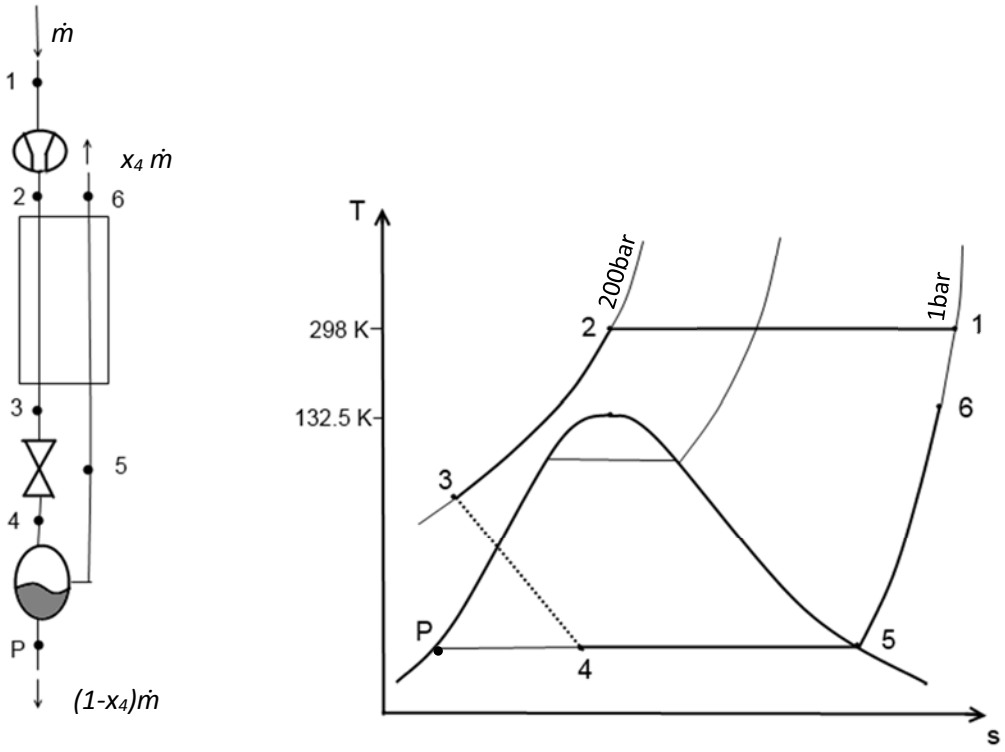


***Figure 5.*** *Linde liquefaction cycle, where 1-2 is ideal isothermal compression, 2-3 isobaric cooling, 3-4 isenthalpic throttling, 4-(P)-5 isothermal separation of liquid fraction, 5-6 isobaric heating and ṁ is the incoming mass flow of air. (Adapted from Struchtrup 2014, p. 278-279)*

A small fraction of the air can also be led to an isenthalpic expander valve and expanded to a lower than atmospheric pressure level, which causes the temperature of the said fraction to drop even further past the boiling point of the air mixture. After this it is led back to the heat exchanger to keep the system cold enough. (Chenier 2002, p. 41-43)

If a simpler one column set-up of the process is used, the liquid air is first injected to the bottom of a fractionating column, where an expander valve is situated. The pressure drops several bars and due to the Joule-Thomson-effect the temperature decreases to -190 °C. Nitrogen has a lower boiling point (-196 °C) than oxygen (-183 °C) and thus the nitrogen remains in gas phase and rises to the top of the column. Oxygen remains in a liquid phase at the bottom of the column, where it can be separated (Chenier 2002, p. 41-43).

For a simple Linde refrigeration process fraction of input air being liquefied $y$ can be calculated from the following equation:

$$y = \frac{h_1 - h_2}{h_1 - h_p} \quad (2.3)$$

where $h_p$ is the specific enthalpy of condensate, $h_1$ is the enthalpy of process output after the heat exchanger and $h_2$ is the enthalpy of process input flow before the heat exchanger. The maximum yield of the process occurs when $h_1$ and $h_2$ are at the same temperature, which is not possible in the actual process. (Flynn 2004, p. 387)

### 2.2.2 Nurmia oxygen enrichment process

The Nurmia oxygen enrichment process has been previously studied in two research studies at the Institute of Energy and Process Engineering of Tampere University of Technology (Saarenpää 2002; Saarenpää et al. 2004). The studies focused on investigating and experimentally verifying the functionality of the basic process and their objective was to prove that the process is possible to be carried out. The process was found operational also in practice. (Saarenpää 2002)

The Nurmia oxygen enrichment process produces oxygen enriched air with a purity of about 50 to 83 % depending on the configuration of the process. The column set-up needs to be contained in thermal insulation, such as a vacuum, in order to keep the process adiabatic. The process principle is illustrated in Figure 6.

The process starts with cooling the slightly compressed and pre-treated air (dashed line in Figure 6) in a heat exchanger almost to the point of condensation (81.5 K in 1 bar). After this, the air is streamed to a separation unit consisting of two nested chambers. First the process air is led through the outermost chamber where oxygen concentrate (red line in Figure 6) condenses. The liquid oxygen concentrate is then throttled to a lower pressure (~0.4 bar), which causes a 4 K temperature drop, and led to the top part of the inner chamber where it evaporates. The heat released in the liquefaction of oxygen in the outer chamber is transferred to the inner chamber where it is consumed by the evaporation of the oxygen concentrate. (Nurmia 2003)

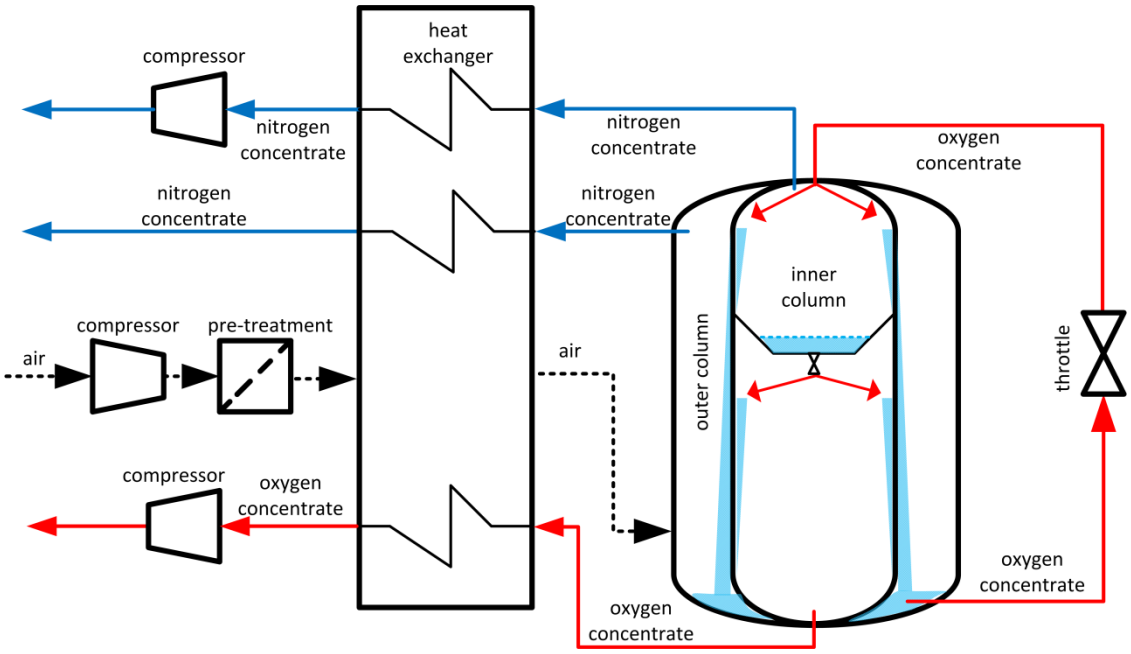


***Figure 6.*** *Simplified Nurmia oxygen enrichment process, where input air (marked with dashed line) is cooled down in a heat exchanger with cold process outputs (oxygen concentrate marked with red line and remaining fraction of air consisting mainly of nitrogen with blue line). Oxygen concentrate forms by condensing in the outer column and is separated and led into the inner column, where it evaporates while consuming heat from the outer column. Finally the gaseous oxygen concentrate is used in heat exchanger to cool down input air. Nitrogen rich remaining fraction of air is led out of both columns in gaseous form and also used in heat exchanger to cool down input air.*

The inner column can also be divided into several sections. In that case, the remaining liquid oxygen concentrate is throttled and evaporated in the lower sections of the inner column. (Nurmia 2003; Saarenpää et al. 2004)

The oxygen concentrate vapor in the inner chamber is finally led out of the process through the heat exchanger and compressor and has a purity of approximately 50-99 %, depending on the process configuration. The gaseous nitrogen (blue line in Figure 6) is also led out of the separation unit and used in heat exchanger to pre-cool the incoming air. The nitrogen from the inner chamber is also compressed back to atmospheric pressure. (Saarenpää 2002; Nurmia 2003)

The process operates near reversibility. The composition of gaseous mixture in equilibrium with liquid depends on the pressure and the temperature. The lower the pressure the higher the oxygen enrichment coefficient there is in the liquid phase. (McKetta 1992, p. 236-237; Nurmia 2003)

The Nurmia oxygen enrichment process has several advantages in comparison to the Linde-Frankl process. Nurmia process operates in nearly normal pressure, so there is less energy needed to compress the air to higher pressure level than in Linde-Frankl

process. Due to the smaller pressure differences, the temperature difference between condensation and evaporation is only 7.5 K, which is considerably less than in Linde-Frankl process, which has a temperature difference of 20 K. Thus the Nurmia process is much closer to reversibility than the Linde-Frankl process. Other advantages of the low pressure level are that it also allows relatively thin and low-cost wall structures to be used in comparison to high pressure processes that require thick, strong and therefore more expensive walls. (Saarenpää 2002; Nurmia 2003)

The Linde-Frankl process operates by liquefying both the oxygen and nitrogen. The Nurmia process only liquefies an oxygen-rich fraction, so there is less energy needed to perform phase transitions. The Nurmia process can be used to produce oxygen with less purity, which is less energy consuming due to smaller separation work. (Saarenpää 2002; Nurmia 2003)

# 3. PROPERTIES OF AIR, OXYGEN AND NITROGEN IN CRYOGENIC CONDITIONS

Several properties of air are illustrated in Figure 7 in an outline of a temperature-entropy diagram for air. Isobars and the saturation curve are plotted in the diagram through a temperature range of approximately 60 to 320 Kelvin.

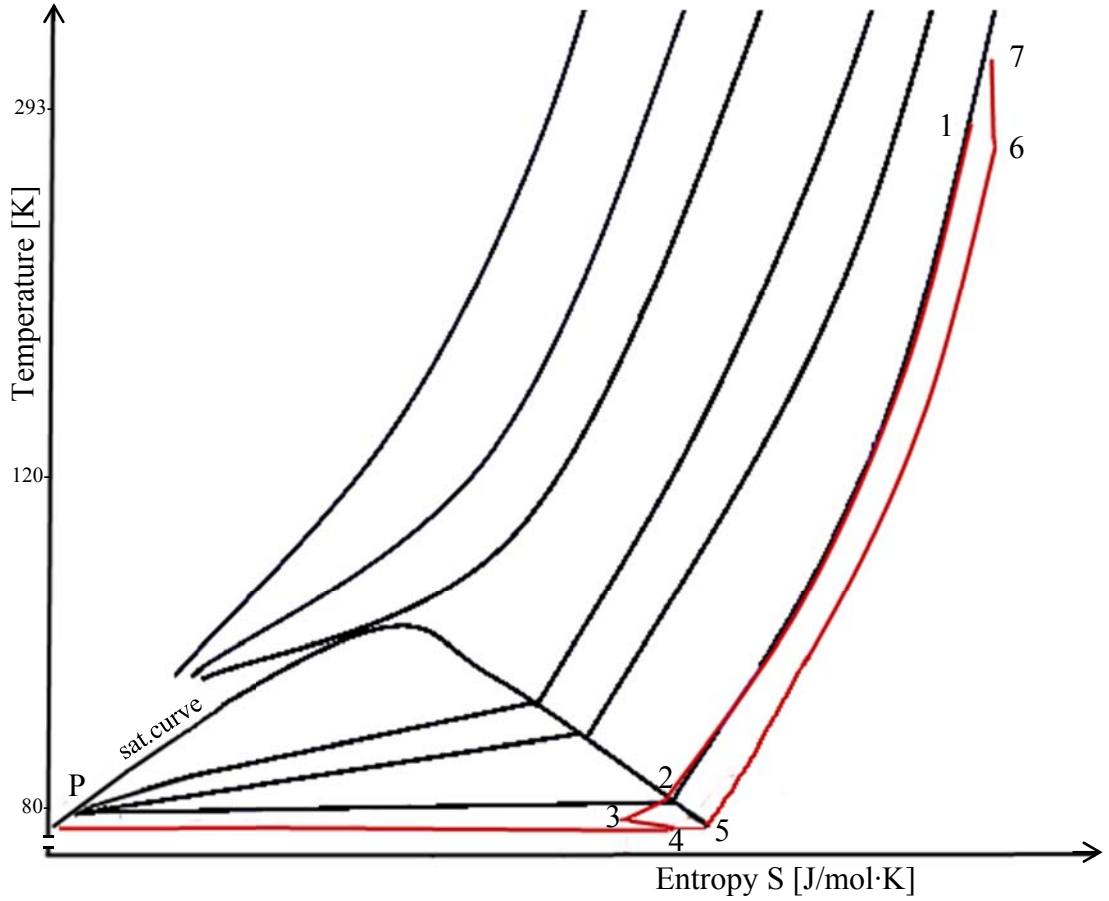


***Figure 7.*** *Outline of a temperature-entropy chart for air with saturation curve and isobars. Nurmia oxygen enrichment process is drawn in red, where stages 1-2 is isobaric cooling, 2-3 condensation in outer column, 3-4 is isenthalpic throttling, 4-P separation of the liquid fraction, 4-5 is evaporation in inner column, 5-6 is isobaric heating and 6-7 is isentropic compression to original pressure level.*

An example of Nurmia oxygen enrichment process is drawn in Figure 7 in red with stages numbered from 1 to 7. Stage 1-2 is the isobaric cooling in heat exchangers, 2-3 is the condensation of oxygen concentrate in the high pressure column, 3-4 is the isenthalpic throttling of oxygen concentrate between columns, 4-P is the separation of the liquid fraction, 4-5 is the evaporation in the low pressure column, 5-6 is the isobaric heating in

heat exchangers and finally stage 6-7 is isentropic compression back to atmospheric pressure. It is important to take into account that under the conditions in this process, the hydrostatic pressure of a liquid column has a substantial effect on the total pressure.

Dry air consists of 78.09 vol-% nitrogen, 20.95 vol-% oxygen, 0.93 vol-% argon, 0.04 vol-% carbon dioxide and small amounts of other components. Air also contains highly variable amounts of water, usually about 0.5-1 vol-% in the form of vapor, depending on the temperature. (Flynn 2004, p. 147)

The physical properties of air are listed in Table 1, where the most important characteristics regarding cryogenic calculations are the normal boiling point at atmospheric pressure, which is -194.3 °C and the latent heat of vaporization, 205 kJ/kg. Other listed characteristics include molecular weight, density and specific volume at normal pressure and temperature, freezing point at atmospheric pressure, critical temperature, critical pressure, critical density, $c_p$, $c_v$, isentropic constant and density of liquid at normal boiling point.

***Table 1.*** *Physical properties of air. (Flynn 2004, p. 146)*

| **Physical constants** | |
|---|---|
| **Molecular weight** | 28,975 g/mol |
| **Density at 21.1 °C and 1 atm** | 1.2000 kg/m$^3$ |
| **Specific volume at 21.1 °C and 1 atm** | 0.8333 m$^3$/kg |
| **Boiling point at 1 atm** | -194.3 °C |
| **Freezing point at 1 atm** | -216.2 °C |
| **Critical temperature** | -140.6 °C |
| **Critical pressure** | 3771 kPa abs |
| **Critical density** | 351 kg/m$^3$ |
| **Latent heat of vaporization at NBP** | 205 kJ/kg |
| **$c_p$ at 21.1 °C and 1 atm** | 1.01 kJ/kg K |
| **$c_v$ at 21.1 °C and 1 atm** | 0.720 kJ/kg K |
| **Isentropic constant ($c_p$/ $c_v$)** | 1.40 |
| **Density of liquid at boiling point, 1 atm** | 874.0 kg/m$^3$ |

Properties of nitrogen in cryogenic temperatures over the range of 65-125 K at a pressure of 1 bar are listed in Table 2. The table includes density, volume, internal energy, enthalpy, entropy, $c_v$, $c_p$, Joule-Thomson coefficient, viscosity, thermal conductivity and phase. The critical temperature for nitrogen is 126.192 K, critical pressure 33.958 bar and critical density 11.1839 mol/l. The normal boiling point is 77.355 K and the standard molecular weight of nitrogen is 28.0134 g/mol. (Span et al. 2000)

***Table 2.*** *Properties of nitrogen in cryogenic temperatures and isobaric pressure of 1 bar. (Span et al. 2000)*

| Temperature [K] | Density [kg/m³] | Volume [l/mol] | Internal Energy [kJ/mol] | Enthalpy [kJ/mol] | Entropy [J/(mol*K)] | $c_V$ [J/mol*K] | $c_P$ [J/mol*K] | Joule-Thomson [K/bar] | Viscosity [µPa*s] | Thermal Cond. [W/m*K] | Phase |
|---|---|---|---|---|---|---|---|---|---|---|---|
| **65.00** | 859.75 | 0.001163 | -4.1202 | -4.1170 | 69.556 | 32.598 | 56.108 | -0.03985 | 280.44 | 0.17322 | liquid |
| **75.00** | 816.73 | 0.001224 | -3.5559 | -3.5525 | 77.632 | 30.762 | 56.892 | -0.03551 | 176.82 | 0.15090 | liquid |
| **77.244** | 806.59 | 0.001239 | -3.4280 | -3.4246 | 79.313 | 30.387 | 57.174 | -0.03418 | 161.37 | 0.14605 | liquid |
| **77.244** | 4.5565 | 0.21947 | 1.5443 | 2.1591 | 151.60 | 21.599 | 31.462 | 2.7169 | 5.4273 | 0.007493 | vapor |
| **85.00** | 4.0942 | 0.24425 | 1.7158 | 2.4000 | 154.57 | 21.311 | 30.722 | 2.2166 | 5.9590 | 0.008288 | vapor |
| **95.00** | 3.6294 | 0.27552 | 1.9324 | 2.7043 | 157.96 | 21.111 | 30.186 | 1.7748 | 6.6327 | 0.009352 | vapor |
| **105.00** | 3.2642 | 0.30635 | 2.1462 | 3.0044 | 160.96 | 21.003 | 29.876 | 1.4671 | 7.2925 | 0.010378 | vapor |
| **115.00** | 2.9683 | 0.33690 | 2.3584 | 3.3022 | 163.67 | 20.938 | 29.682 | 1.2412 | 7.9385 | 0.011360 | vapor |
| **125.00** | 2.7229 | 0.36725 | 2.5695 | 3.5983 | 166.14 | 20.898 | 29.552 | 1.0688 | 8.5708 | 0.012307 | vapor |

Table 3 includes the properties of oxygen at cryogenic temperatures over the range of 55 to 125 K at a pressure of 1 bar. The table contains density, volume, internal energy, enthalpy, entropy, $c_v$, $c_p$, Joule-Thomson coefficient, viscosity, thermal conductivity and phase.

***Table 3.*** *Properties of oxygen at cryogenic temperatures and isobaric pressure of 1 bar. (Schmidt & Wagner 1985; Laesecke et al. 1990)*

| Tem-perature [K] | Density [kg/m³] | Volume [l/mol] | Internal Energy [kJ/mol] | Enthalpy [kJ/mol] | Entropy [J/mol*K] | $c_V$ [J/mol*K] | $c_P$ [J/mol*K] | Joule-Thom-son [K/bar] | Viscosity [µ Pa*s] | Thermal Cond. [W/m*K] | Phase |
|---|---|---|---|---|---|---|---|---|---|---|---|
| **55.000** | 1303.6 | 0.00076 | -6.1617 | -6.1592 | 67.563 | 37.644 | 53.478 | -0.03789 | 873.53 | 0.20011 | liquid |
| **65.000** | 1259.8 | 0.00079 | -5.6263 | -5.6238 | 76.507 | 33.473 | 53.662 | -0.03632 | 499.33 | 0.18745 | liquid |
| **75.000** | 1214.0 | 0.00082 | -5.0895 | -5.0869 | 84.190 | 31.750 | 53.712 | -0.03498 | 322.60 | 0.17351 | liquid |
| **85.000** | 1166.7 | 0.00085 | -4.5514 | -4.5487 | 90.926 | 30.368 | 54.007 | -0.03286 | 228.18 | 0.15917 | liquid |
| **90.062** | 1141.8 | 0.00087 | -4.2773 | -4.2745 | 94.060 | 29.738 | 54.367 | -0.03128 | 196.51 | 0.15180 | liquid |
| **90.062** | 4.4135 | 0.22658 | 1.8220 | 2.5470 | 169.80 | 21.622 | 31.056 | 2.3613 | 7.0032 | 0.00835 | vapor |
| **95.000** | 4.1642 | 0.24014 | 1.9290 | 2.6974 | 171.43 | 20.955 | 30.120 | 2.0325 | 7.3736 | 0.00883 | vapor |
| **105.00** | 3.7418 | 0.26725 | 2.1417 | 2.9969 | 174.43 | 20.909 | 29.861 | 1.7033 | 8.1178 | 0.00978 | vapor |
| **115.00** | 3.4001 | 0.29411 | 2.3539 | 3.2950 | 177.14 | 20.939 | 29.752 | 1.4592 | 8.8525 | 0.01073 | vapor |
| **125.00** | 3.1174 | 0.32078 | 2.5655 | 3.5919 | 179.61 | 20.929 | 29.638 | 1.2596 | 9.5765 | 0.01168 | vapor |

The critical temperature for oxygen is 154.581 K, critical pressure 50.430 bar and critical density 13.63 mol/l. Its normal boiling point is 90.1878 K. The standard molecular weight of oxygen is 31.9988 g/mol. (Schmidt & Wagner 1985; Laesecke et al. 1990)

# 4. MODELLING OF SUBPROCESSES IN OXYGEN ENRICHMENT PROCESS

The Nurmia oxygen enrichment process consists of several stages. Noteworthy subprocesses occurring in the Nurmia oxygen enrichment process and related process components are studied below.

## 4.1 Pre-treating of air

The air is pre-treated in order to remove the components that can disturb the enrichment process, such as water vapor, carbon dioxide and particles. The principle of the pre-treatment process is illustrated in Figure 8. Pre-treating of air causes pressure losses and increases the compressor duty. Pre-treating processes involving refrigeration also need energy to run the refrigeration process.

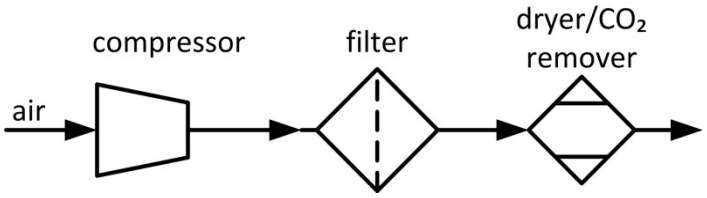


***Figure 8.*** *Pre-treatment process of air including filtering to remove particles, dryer and $CO_2$ remover.*

The air is first filtered in order to remove particles. The drying of air can be done by cooling in a refrigeration system, where the humidity freezes and carbon dioxide condenses. Other ways to remove water vapor, carbon dioxide and other gaseous components include molecular sieves, a regenerator or a suitable absorbent. (Castle 2002, p. 160)

A pre-treatment process to remove water and carbon dioxide involving molecular sieves is illustrated in Figure 9. Molecular sieves work by adsorbing for example water and carbon dioxide molecules in their pores while letting other molecules pass through. The air is first compressed and cooled down before streaming it to the molecular sieve absorbers interconnected through a valve assembly. The sieves are cooled with cold nitrogen product from the air separation process. (Castle 2002, p. 160; Linde engineering 2009, p. 14; Fu & Gundersen 2012, p. 65-66)

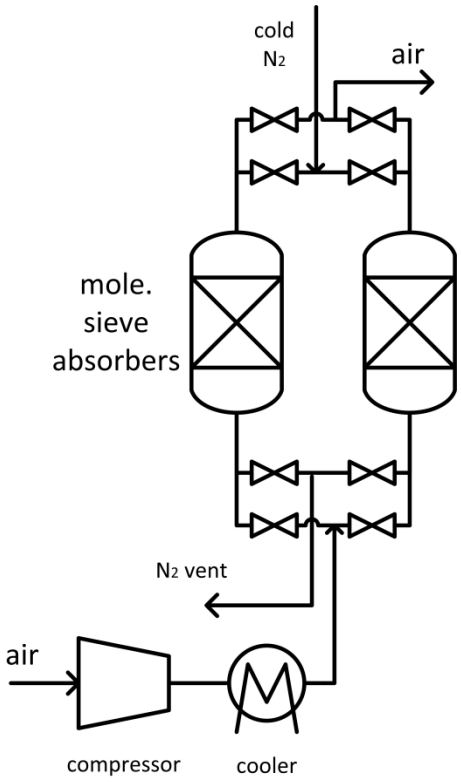


***Figure 9.*** *Pre-treatment process of air using molecular sieve absorbers (Adapted from Castle 2002, p. 160)*

In comparison to Linde-Frankl process, in Nurmia method the removal of moisture and $CO_2$ has to be more thorough. This is due the fact that in Linde-Frankl method moisture and $CO_2$ will condense or freeze in the regenerator and can be removed with a reverse flow and consequently at least some can be left in the process air. (Nurmia 2003)

## 4.2 Pre-cooling of air in heat exchanger

In the heat exchange process of Nurmia oxygen enrichment method, the inputs are the input air being cooled down, the two cold nitrogen concentrates and the oxygen concentrate product being led out of the process. All the four streams are in the vapor phase. The air cools down in the heat exchanger to almost the point of condensation. In the pressure of 1 bar the temperature in question is 81.5 K (Nurmia 2003). Heat flow $\dot{Q}$ in a closed well insulated heat exchanger can be derived from the conservation of mass and energy:

$$\dot{Q} = \dot{m}_H\left(h_{H,i} - h_{H,o}\right) = \dot{m}_C\left(h_{C,o} - h_{C,i}\right) \qquad (4.1)$$

where $\dot{m}$ is mass flow of a stream through the heat exchanger, $h_i$ the enthalpy before and $h_o$ after the heat exchanger. The subscripts $H$ and $C$ refer to hot and cold streams respectively (Mills 1999, p. 658; Struchtrup 2014, p. 200).

If specific heat can be assumed constant within the scale of the process, enthalpy can also be presented $dh = c_p dT$, where $c_p$ is specific heat and T is temperature. On this condition the equation (4.1) can also be written as follows (Mills 1999, p. 659):

$$\dot{Q} = (\dot{m}c_p)_H\left(T_{H,i} - T_{H,o}\right) = (\dot{m}c_p)_C\left(T_{C,o} - T_{C,i}\right) \qquad (4.2)$$

Figure 10 illustrates the principle of a simple counter-current heat exchanger, where hot input with a temperature of $T_{H,i}$ flowing in the outer tube heats up the cold input $T_{C,i}$ flowing in the nested inner tube to a temperature of $T_{C,o}$. The hot input cools down to $T_{H,o}$.

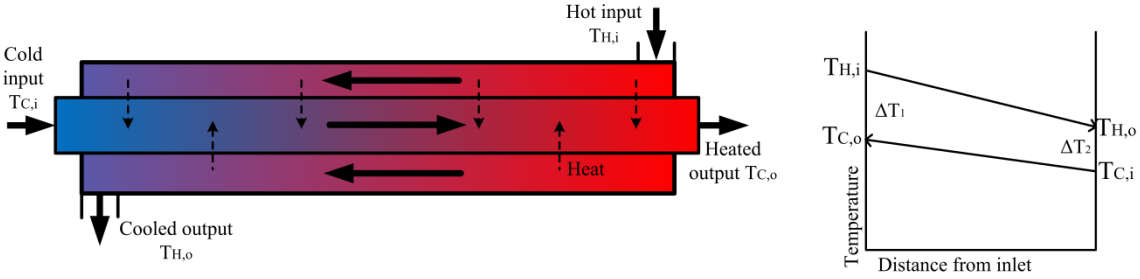


***Figure 10.*** *Simplified counterflow heat exchanger and a temperature profile over the heat exchanger operating adiabatically in constant phase. Hot input heats up the cold input through heat exchange over the heat-exchange surface between the separate flows. Black arrows represent the direction of flow and dotted arrows represent the direction of heat exchange.*

Heat transfer from stream to another and pressure drop over the heat exchanger cause irreversibility to the heat exchange process. Exergy losses can be decreased by keeping the temperature differences between the hot and cold stream as small as possible and by minimizing pressure drop over the heat exchanger. (Cornelissen & Hirs 1997)

Effectiveness $\varepsilon$ for heat exchanger can be presented with following equation:

$$\varepsilon = \frac{actual\ energy\ transfer}{maximum\ energy\ transfer} \qquad (4.3)$$

where actual energy transfer is the energy that has transferred from the hot stream to the cold stream and maximum energy transfer is the theoretical maximum value of said energy (Flynn p. 390-391).

**APPLICABLE HEAT EXCHANGER TYPES**

The Nurmia oxygen enrichment process requires efficient heat exchangers in order to minimize or prevent the need of using additional refrigeration in the process. Both regenerators and recuperators can be used to carry out the heat exchange process between input air and the cold feeds. A suitable recuperator for the process could for example be a spiral heat exchanger consisting of three flat sheets coiled forming two separate counter-current flow passages and closed sides. (Nurmia 2003)

A regenerative heat exchanger operates by periodically alternating hot and cold flows through a regenerative matrix which stores and releases heat (Mills 1999, p. 654; Flynn 2004, p. 401). A suitable regenerator type for the Nurmia oxygen enrichment process could be for example a pebble heat exchanger with mechanical conveying (McKetta 1992, p. 325–329). Though it has to be noted that normally a regenerator can only operate using two streams. Thus in Nurmia process, each of the three cold streams would have to be directed to their own regenerators with an equivalent fraction of the warm input air as the warm stream.

The advantages of using a regenerator are that a regenerator is self-cleaning and has a small pinch-point temperature difference. It can be situated around the process apparatus and thus function as a cold box. At low pressure levels the regenerator does not need to have an airtight structure either so the seams need no welding. (McKetta 1992, p. 101-102)

## 4.3 Condensation of oxygen in the high pressure column

Condensation on the separating wall of the outer high pressure column and inner low pressure column is due to the heat exchange between the columns. The condensation takes place when the cold oxygen gas comes into contact with a surface at lower temperature. The evaporation of oxygen concentrate occurring in the inner low pressure column consumes heat, which is conducted from the outer high pressure column through the separating wall. The temperature difference between the two columns is relatively small because the separating wall operates as an evaporator on one side and a condenser on the other, as illustrated in Figure 11. (McKetta 1992, p. 236-247)

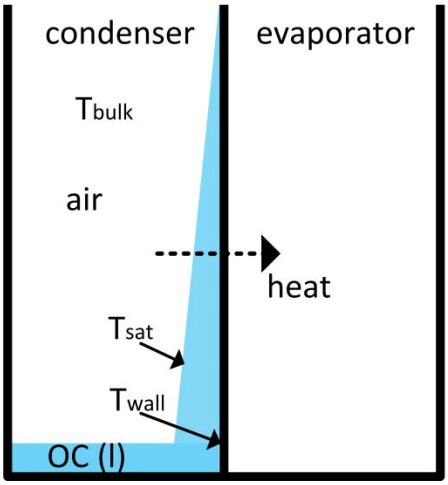


***Figure 11.*** *Principle of the condensation of oxygen on the cold separating wall between condenser and evaporator, where blue represents the condensed liquid product (OC). Evaporation consumes heat which is conducted through the separating wall.*

The liquid continuously flows downward and therefore the layer thickness increases steadily along the height of the vertical condensing surface, as seen in Figure 11 (McKetta 1992, p. 9). The flow in the vertical falling film is usually laminar, on the condition that the condensation rate is not especially high (Mills 1999, p. 572).

Stefan flow is a convective flow caused by the removal or production of gas at an interface. The removal or production can be due to either chemical reaction or phase change. It causes a suction effect on the vapor boundary layer when liquid condenses on a surface. The suction increases vapor drag and heat transfer from the vapor. (Mills 1999, p. 601; Kolev 2011, p. 342-345)

The condensation process can be either film condensation or dropwise condensation. If the liquid wets the surface it is called film condensation and if the liquid only forms droplets it is called dropwise condensation. Usually during the initial starting of a condenser the condensation is first dropwise but eventually develops to film condensation. Therefore a film condensation should usually be presumed in heat transfer estimation. (McKetta 1992, p. 9; Mills 1999, p. 571-572)

Condensate mass flow $\dot{m}$ in the process illustrated in Figure 11 can be calculated when the latent heat of condensation $h_{fg}$ and the heat transfer $\dot{Q}$ across the surface is known. The heat transfer $\dot{Q}''$ per area is constant through the interface, the film and the wall and thus can be calculated by the means of the following relation:

$$\dot{m} = \frac{\dot{Q}}{h_{fg}} = \frac{\bar{h}A(T_{sat}-T_w)}{h_{fg}}; \qquad (4.4)$$

$$\dot{Q}'' = k\frac{(T_{sat}-T_w)}{\delta} \qquad (4.5)$$

where $T_w$ is the wall temperature, $T_{sat}$ is the saturation temperature, $A$ is the area where condensation occurs, $k$ is the thermal conductivity of the condensate layer and $\delta$ is the condensate layer thickness. (Bayazitoglu & Özisik 1988, p. 309-310; Mills 1999, p. 574–575)

The transition from laminar to turbulent flow occurs when the Reynolds number reaches approximately 1800. The Reynolds number for liquid flow over a vertical surface is defined below, and by introducing equation (4.4) it can also be expressed in another way:

$$Re = \frac{4\dot{m}}{\mu_l P} = \frac{4A\bar{h}(T_{sat}-T_w)}{h_{fg}\mu_l P} \qquad (4.6)$$

where $\dot{m}$ is the mass flow of condensate at the bottom of the surface and $P$ is the wetted perimeter. (Bayazitoglu & Özisik 1988, p. 306–310)

The local heat transfer coefficient $h$ for laminar film condensation on a vertical wall is

$$h = \left[\frac{g\rho_l(\rho_l-\rho_v)h_{fg}k_l^3}{4x\mu_l(T_{sat}-T_w)}\right]^{1/4} \qquad (4.7)$$

where $g$ is the gravitational acceleration, $h_{fg}$ is the latent heat of condensation, $k_l$ is the thermal conductivity of liquid, $x$ is the position along the height of condenser, $\rho_l$ and $\rho_v$ are the density of liquid and vapor, $\mu_l$ is the viscosity of liquid and $T_{sat}$ and $T_w$ are the saturation temperature of vapor and wall temperature. (Mills 1999, p. 577)

The average heat transfer coefficient $\bar{h}$ can be defined using the local heat transfer coefficient by integrating

$$\bar{h} = \frac{1}{L}\int_0^L h(x)dx \qquad (4.8)$$

where $L$ is the length of the plate (Faghri & Zhang 2006, p. 608).

A correlation of average heat transfer coefficient $\bar{h}$ for condensation on a vertical surface at constant temperature and with slow or stagnant flow of vapor is presented below. The correlation is an improved version of the Nusselt equation for condensation on vertical surface that can be derived from equation (4.7). Equation (4.9) has been altered to correspond better to experimentally measured values of heat transfer coefficient. Fluid properties are considered constant and heat transfer across the liquid layer is considered linear. Correlation (4.9) is for laminar flow of condensate and correlation (4.10) is for turbulent flow of condensate.

$$\bar{h} = 1.13\left[\frac{g\rho_l(\rho_l-\rho_v)h_{fg}k_l^3}{\mu_l(T_{sat}-T_w)L}\right]^{1/4} \text{ for Re} < 1800 \qquad (4.9)$$

$$\bar{h} = 0.0077 Re^{0.4} k_l \left(\frac{g\rho_l^2}{\mu_l^2}\right)^{1/3} \text{ for Re } > 1800 \qquad (4.10)$$

where physical properties are evaluated at the film temperature $T_f = \frac{1}{2}(T_w - T_{sat})$ and $L$ is the length of the surface. (Bayazitoglu & Özisik 1988, p. 304–311; Mills 1999, p. 577, Faghri & Zhang 2006, p. 608)

A more exact solution for local heat transfer coefficient for condensation that takes vapor velocity also into account is

$$h = \left[\frac{k_l^2 U_e}{8\nu_l x}\left\{1 + \left(1 + \frac{16 Pr_l}{Ja_l}\frac{gx}{U_e^2}\right)^{1/2}\right\}\right]^{1/2} \qquad (4.11)$$

where $U_e$ is the vapor velocity, $\nu_l$ is the kinematic viscosity of liquid, $Pr$ is the Prandtl number and $Ja$ is the Jakob number. Equation (4.11) is valid when $\rho_v \ll \rho_l$ and $U_\delta \ll U_e$, where $U_\delta$ is the velocity of film surface. (Mills 1999, p. 592–595)

However, the presence of noncondensing nitrogen causes a need for special consideration regarding the mathematical modelling of the process in the outer column of Nurmia oxygen enrichment method. The effect of noncondensing fraction to the condensation is studied in the following chapter.

## CONDENSATION OF OXYGEN IN THE PRESENCE OF NON-CONDENSING NITROGEN

In Nurmia oxygen enrichment process the condensation of oxygen enriched air occurs in the presence of a noncondensing component, nitrogen (Nurmia 2003). Hence the rate of condensation and heat transfer is not only controlled by convection, but also by diffusion of oxygen through the noncondensing nitrogen.

Noncondensable gas in vapor potentially greatly reduces the heat transfer coefficient. This is due to the fact that when the vapor condenses on a surface the noncondensing fraction of the mixture accumulates at the surface, as illustrated in Figure 12. The condensing vapor has to diffuse through the noncondensing gas in order to reach the condensing surface. This causes a resistance to vapor and thus a drop of the partial pressure of the condensing vapor, as seen in Figure 12. Hence the temperature of the condensate layer is lower than the bulk saturation temperature, which is also shown in Figure 12. However, the accumulation of noncondensing gas can be reduced with vapor flow pattern adjustments, such as higher velocities of vapor over the condensing surface. (Bayazitoglu & Özisik 1988, p. 315; Panzarella & Kassemi 2009)

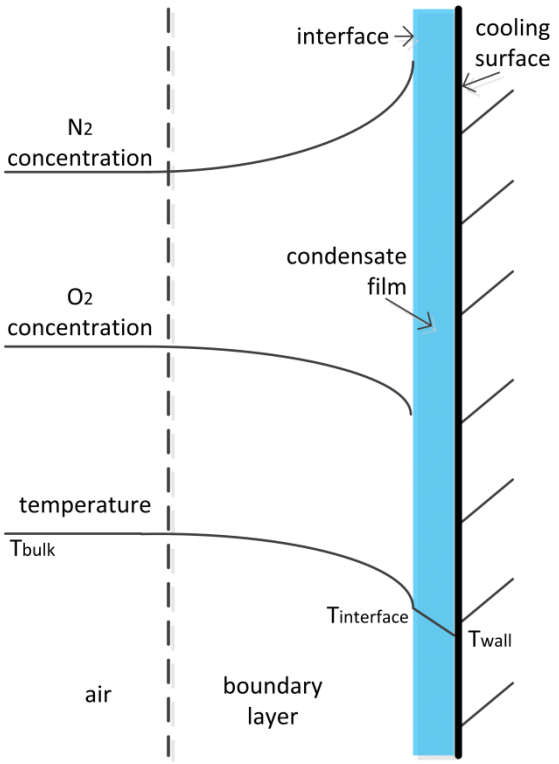


***Figure 12.*** *Formation of a diffusion boundary layer containing non-condensing nitrogen during condensation of oxygen. The concentration of non-condensing nitrogen increases and the concentration of oxygen decreases at the boundary layer. The temperature decreases in the boundary layer and in the condensate layer.*

The accumulation of noncondensing gas at the surface continues until the increasing concentration gradient is able to generate a diffusive flux equal and opposite to the kinetic flux caused by Stefan flow (Mills 1999, p. 831). The molar condensation rate $\dot{N}_A''$ per area of the condensing surface can be derived from Fick's law of binary diffusion (Mills 1999, p. 754), where the condensation rate for noncondensable gas $\dot{N}_B''$ is zero:

$$\dot{N}_A'' p_B = \frac{pD}{RT}\frac{dp_B}{dz} \tag{4.12}$$

where $p_B$ is the partial pressure of noncondensable gas, $p$ is the total pressure, $D$ is the diffusion coefficient, $R$ is the gas constant and $T$ the temperature. The partial pressure of the noncondensable gas at the boundary layer $p_{Bi}$ can be presented:

$$p_{Bi} = p_{Bb} e^{RTN_A'' \delta / pD} \tag{4.13}$$

where $p_{Bb}$ is the partial pressure of noncondensable gas in the bulk and $\delta$ is the thickness of the laminar film (Kay & Nedderman 1985, p. 526-527).

The total pressure of a vapor-gas mixture $p_t$ can be calculated using Dalton's law as a sum of partial pressures, on the condition that ideal gas behavior occurs,

$$p_t = p_v + p_g \tag{4.14}$$

where $p_v$ is the partial pressure of oxygen and $p_g$ is the partial pressure of the non-condensing nitrogen of the mixture (Shavit & Gutfinger 2009, p. 339).

From the equation of state for ideal gases we get the following equations of state for the vapor and gas phases. The temperatures of vapor and gas are considered equal.

$$p_v = \frac{m_v R T_v}{M_v V_v} = \frac{R T_v \rho_v}{M_v} \tag{4.15}$$

$$p_g = \frac{m_g R T_g}{M_g V_g} = \frac{R T_g \rho_g}{M_g} \tag{4.16}$$

where $p$ is pressure, $R$ is the universal gas constant, $T$ is temperature of the gas, $V$ is volume, $M$ is molar mass and $\rho$ is density. (Shavit & Gutfinger 2009, p. 84)

The Colburn-Hougen method can also be used to evaluate condensation in the presence of non-condensable gas. It is based on the energy conservation principle, requiring that the rate of sensible heat transfer through the non-condensing gas film is equal to the latent heat transferred through the condensate and the tube. The interface pressure and temperature can be solved by iteration from the energy balance equation, thus solving the heat transfer rate. The Colburn-Hougen equation is presented below:

$$h_g(T_g - T_i) + k_m h_{fg}(c_v - c_{vi}) = h_c(T_i - T_c) \tag{4.17}$$

where $h_g$ is the heat transfer coefficient for the non-condensing gas film and $T_g$ and $T_i$ are the temperatures of bulk gas and the interface, respectively. In the equation $k_m$ is the mass transfer coefficient, $h_{fg}$ is the latent heat of condensing vapor, $c_v$ and $c_{vi}$ are the molar concentrations of condensing vapor per volume in the bulk gas and in the interface respectively, $T_c$ is the temperature of the condensate and $h_c$ is the heat transfer coefficient for the condensate layer. Using equation (4.17) the interface pressure and temperature can be determined by iteration. (Colburn & Hougen 1934)

The heat flux through the boundary layer is measured through the difference of the non-condensable partial pressures at the bulk and the interface divided by the logmean of these partial pressures:

$$\dot{Q}_v'' = \dot{m}_g'' h_{fgb} = k_m h_{fgb} \rho_{vb} \ln\left(\frac{1 - \frac{p_{vi}}{p}}{1 - \frac{p_{vb}}{p}}\right) \tag{4.18}$$

where $\dot{m}_g''$ is the mass flux of gas, $h_{fgb}$ is the evaporation latent heat at the partial pressure of oxygen in the bulk, $\rho_{vb}$ is the density of the vapor bulk, $p_{vi}$ and $p_{vb}$ are the partial pressures of vapor at the interface and in the bulk respectively, and $p$ is the total pressure. (Colburn & Hougen 1934; Bang et al. 2009)

## 4.4 The effect of pressure and temperature on the equilibrium composition of oxygen-nitrogen mixtures

The equilibrium composition of a liquid oxygen concentrate depends on its temperature and pressure. In Nurmia oxygen enrichment process the liquid and gas are in equilibrium at each process stage and no significant dissolution occurs (Nurmia 2003). However, in cases where liquid oxygen is in contact with air, solubility of nitrogen is notable and has to be considered. This can occur if there are air leaks in the system. Therefore the air tightness of the system is important. The effect of total pressure to the equilibrium concentration of the liquid oxygen-nitrogen solution is also important to consider because of the pressure level of the process affects the enrichment coefficient of oxygen during the process, as discussed in Chapter 2.2.2.

For ideal solutions in low pressures, the solubility of gas can be calculated using Raoult's law for a single component:

$$x_i = \frac{p}{p_i} \tag{4.19}$$

where $x_i$ is the mole fraction of the solute gas i in solution, $p$ is the partial vapor pressure of the component i in the gaseous phase and $p_i$ is the vapor pressure of pure component i. (Shavit & Gutfinger 2009, p. 504-505; Mersmann et al. 2011, p. 29-30)

Usually solutions do not behave ideally over different values of properties (Shavit & Gutfinger 2009). Zimmerli et al. have presented a correlation for the nitrogen mole fraction in nitrogen-oxygen mixtures in the proximity of the boiling temperature of oxygen depending on pressure and temperature (Zimmerli et. al 2010).

$$x_{N_2} = g(T) \cdot p^* + h(T) \cdot p^{*2} \tag{4.20}$$

where p$^*$ is dimensionless pressure defined as $p^* = \frac{p - p_0^{O_2}}{p_0^{N_2}}$, where $p$ is total pressure, $p_0^{O_2}$ and $p_0^{N_2}$ are the saturated vapor pressures of oxygen and nitrogen respectively, and $g$ and $h$ are coefficients defined below:

$$g(T) = 1.3114 - \frac{0.0148}{K} \cdot T + \frac{1.6 \cdot 10^{-4}}{K^2} \cdot T^2 \tag{4.21}$$

$$h(T) = 0.70 - \frac{0.006}{K} \cdot T \tag{4.22}$$

where $T$ is the temperature in Kelvin and $K$ is the temperature unit Kelvin. Zimmerli et al. gives a value of 1.3 % for standard deviation of data to correlation (Zimmerli et al. 2010). The solubility of nitrogen in liquid oxygen is plotted as mole fraction of nitrogen $x_{N2}$ in liquid phase in Figure 13:

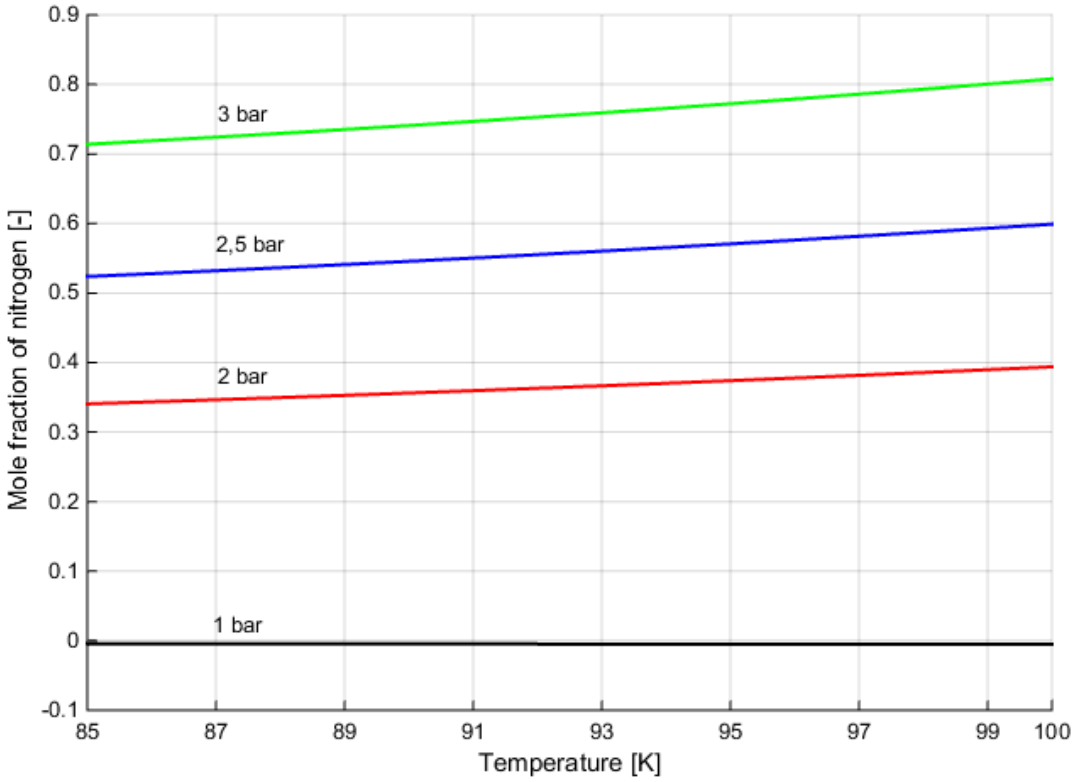


***Figure 13.*** *The mole fraction of gaseous nitrogen $x_{N2}$ dissolved in liquid oxygen in equilibrium as a function of temperature at different pressure levels.*

From Figure 13 can be seen that the solubility of gaseous nitrogen in liquid oxygen increases significantly when the pressure level is increased. Therefore a contamination of oxygen in the diffusion layer between the two phases can be expected while using higher than atmospheric pressure levels, if a leak of air to the process occurs. However, the contamination process is very slow if the only mixing mechanism is diffusion. (Zimmerli et al. 2010)

Without any additional mixing taking place between the liquid and gaseous phases, such as stirring or convection, the contamination of oxygen occurs due to the diffusion of nitrogen into the liquid oxygen. The concentration of solute (nitrogen) in liquid solvent (oxygen) at certain point of time and at a flat one-dimensional interface can be estimated using a function derived from the Fick's second law:

$$c(y,t) = c_0 \cdot \mathrm{erfc}\left(\frac{\delta}{2\sqrt{D_{AB}t}}\right), \qquad (4.23)$$

where $c_0$ is the equilibrium concentration of solute at the interphase, erfc*(x)* is the complementary error function, δ is the distance from the interface, $D_{AB}$ is the diffusivity of solute in the solvent in question and *t* is the time. (Zimmerli et al. 2010)

For the diffusivity of nitrogen in liquid oxygen at 90 K, Zimmerli et al. use the value of $D_{AB} = 5 \cdot 10^{-5}$ cm$^2$/s. Equation (4.23) can be used to evaluate the location δ of the diffu-

sion front when a 1 % of the equilibrium concentration value has been reached. Thus the concentration values can be reduced from the equation (4.23) and it becomes $0.01 = \mathrm{erfc}\left(\frac{\delta}{2\sqrt{D_{AB}t}}\right)$. Using an error value table (Mills 1999, p. 968) the equation gives $\delta = 3.64 \cdot (D_{AB}t)^{0.5}$. For example after two hours, i.e. t = 7200 s the δ = 2.2 cm. From this can be concluded that mixing only by diffusion is slow. (Zimmerli et al. 2010)

## 4.5 Throttling of oxygen concentrate

In the Nurmia oxygen enrichment process the liquid oxygen concentrate is throttled to a lower pressure level (Nurmia 2003). The operating principle of throttling device is to create a pressure drop by streaming the fluid through a restraint, such as a small orifice or porous matter. The high friction losses make throttling irreversible. This isenthalpic pressure drop causes a decrease in the temperature of the concentrate due to the Joule-Thomson effect. (Flynn 2004, p. 369; Struchtrup 2014, p. 188)

Joule-Thomson coefficient $(\partial T/\partial p)_h$ determines if the isenthalpic pressure drop causes an increase or a decrease in the temperature. A positive Joule-Thomson coefficient causes a reduction in the temperature when the gas is expanded. The Joule-Thomson coefficient can be plotted in order to draw an inversion curve for real gases, as seen in Figure 14, where inversion curves for helium, hydrogen, air, argon, carbon dioxide and ammonia are plotted. At temperature and pressure levels below the inversion curve, a pressure drop also decreases the temperature. On the other hand at temperature and pressure levels above the inversion curve, a pressure drop increases the temperature. (Flynn 2004, p. 369-370; Struchtrup 2014, p. 387)

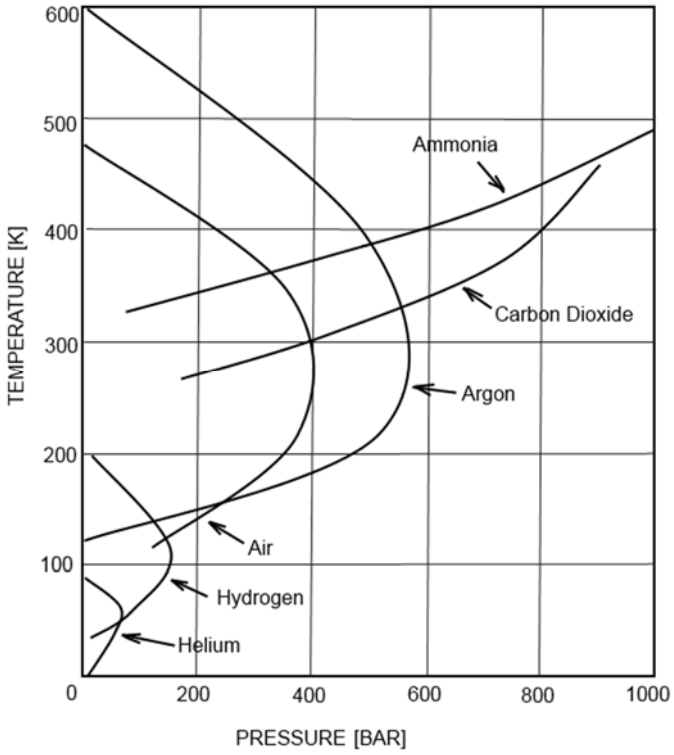


***Figure 14.*** *Inversion curves for helium, hydrogen, air, argon, carbon dioxide and ammonia. A pressure drop causes a temperature drop to a gas if its temperature and pressure are below the inversion curve of the gas. (Adapted from Flynn 2004, p. 371)*

Isentropic expansion engines, such as turbines, could potentially provide better efficiency for the process than simple throttles. Unfortunately they are difficult to use in gas liquefaction processes because the liquid fraction of the stream causes erosion in the turbine. Therefore throttles are usually used as primary expansion devices in such processes. (Flynn 2004, p. 369)

## 4.6 Evaporation of oxygen concentrate in the low pressure column

In the Nurmia process the oxygen concentrate is evaporated in the low pressure column after throttling in order to absorb heat from the high pressure column, as illustrated in Figure 15. Configuration of the process determines whether evaporation or boiling occurs. Usually the process type in low pressure column is evaporation on the surface of the liquid film, because the wall temperature is not high enough to cause boiling in the liquid layer. Increased mass flow of oxygen concentrate leads to higher temperature of the separating wall and even boiling might occur (Nurmia 2003).

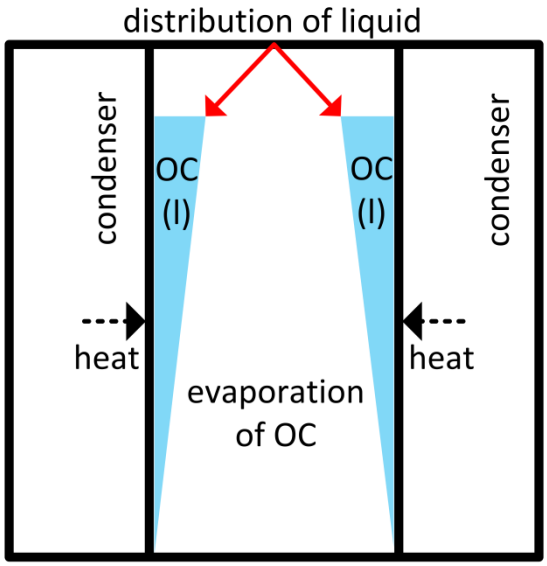


***Figure 15.*** *Evaporation of liquid oxygen concentrate (OC) is carried out by distributing and creating a falling film on the surrounding condenser walls and by using the heat from the condenser.*

The latent heat of oxygen at normal boiling point is 0.213 MJ/kg. (Mills 1999, p. 925) First the oxygen concentrate is distributed evenly inside the column from an isenthalpic spray nozzle at the top of the inner column. The evaporation takes place on the vertical separating wall between the inner and outer columns. The inner column can also consist of several stages, each with means where the remaining liquid fraction of the oxygen concentrate is gathered and then again throttled and sprayed in order to achieve a complete evaporation of the liquid. (Nurmia 2003)

The falling film of liquid easily withdraws from the column walls, which leads to dryout and therefore a sharp decline in the heat flux. The withdrawal from the surface can potentially be prevented or delayed by using improved boiling surfaces, such as roughened, finned or porous surfaces. (McKetta 1992, p. 28–30)

Evaporation is a mass transfer process that occurs when the saturation pressure at the temperature of the interface is greater than the vapor pressure. The evaporation occurs on the separating wall between the two columns. A wall temperature that is higher than the saturation temperature of a liquid causes superheating of the liquid close to the wall. If the superheat is high enough, boiling follows and thus the falling film will be dispersed complexing heat transfer processes. Film evaporation creates vapor at the surface of the liquid film but boiling generates vapor also inside the liquid. (Mills 1999, p. 599 & p. 603–607; Faghri & Zhang 2006, p. 683)

Stefan flow, which is a flow caused by the removal or production of vapor volume at an interface, causes a blowing effect on the vapor boundary layer. The blowing reduces

vapor drag and heat transfer to the vapor. However when evaporation rate is high enough, the effect can be insignificant. (Mills 1999, p. 599-601; Kolev 2011, p. 342-345)

The Reynolds number Re for a mass flow rate per surface width can be defined

$$\mathrm{Re} = \frac{4\Gamma}{\mu_l} \tag{4.24}$$

where mass flow rate $\Gamma$ per unit width is

$$\Gamma = \int_0^{\delta} \rho_l u dy \tag{4.25}$$

where δ is the film thickness, $\rho_l$ is the density of liquid and $u$ is the velocity of flow. The film thickness of an evaporating laminar film can be solved:

$$\delta = \left[\frac{3\mu_l \Gamma}{\rho_l(\rho_l - \rho_v)g}\right]^{1/3} \tag{4.26}$$

Because the heat transfer through the evaporating film is due to conduction only, the local heat transfer coefficient is

$$h_x = k_l/\delta \tag{4.27}$$

where $k_l$ is the conductivity of liquid. (Mills 1999, p. 599-601; Faghri & Zhang 2006, p. 702-704; Mersmann et al. 2011, p. 131-132)

If the temperature of the heated wall is high enough, nucleate boiling occurs. This reduces the heat flux between the wall and the liquid, because the vapor film covers the wall and thus the liquid is separated from the surface. (Mills 1999, p. 605)

For film boiling of a cryogenic liquid on a vertical surface with turbulent flow an average heat transfer coefficient $\bar{h}$ can be written as

$$\bar{h} = 0.15\left[\frac{(\rho_l - \rho_v)g h'_{fg} k_v^2}{\nu_v (T_w - T_{sat})}\right]^{\frac{1}{3}} \quad \text{when} \quad \frac{L^3(\rho_l - \rho_v)g h'_{fg}}{k_v \nu_v (T_w - T_{sat})} > 5 \times 10^7 \tag{4.28}$$

where modified latent heat $h'_{fg} = h_{fg} + 0.50 c_{pv}(T_w - T_{sat})$ and $L$ is the length of the film. The subscript *l* refers to liquid, *v* to vapor, *w* to wall and *sat* to saturation. (Mills 1999, p. 615)

## 4.7 Compression of nitrogen and oxygen concentrates

The nitrogen and oxygen concentrates that come from the inner column are at a lower than atmospheric pressure level. After the heat exchanger they are compressed back to atmospheric pressure in order to maintain the flow in the process. After the heat exchanger, all of the streams are in gaseous phase (Nurmia 2003). Thus the following equation for theoretical compression power $P_s$ [kW] can be used, assuming ideal gas behavior and isentropic compression:

$$P_s = \dot{m}\Delta h_s = \dot{m} \int \nu dp = \dot{m} \frac{c_p}{\gamma} T_1 \left[ \left( \frac{p_2}{p_1} \right)^{\frac{\gamma-1}{\gamma}} - 1 \right] \qquad (4.29)$$

where $\dot{m}$ is the mass flow rate [kg/s], $\Delta h_s$ is the isentropic enthalpy change, $\nu$ is the specific volume, $c_p$ is the specific heat capacity, $\gamma$ is the isentropic constant and $p_1$ and $p_2$ are the pressures before and after the compressor respectively. (Fu & Gundersen 2012; Raiko 2013, p. 2-3; Raiko & Saarenpää 2014, p. 10)

For a real compression process the compression power $P$ [kW] is

$$P = \frac{P_s}{\eta_s} \qquad (4.30)$$

where $\eta_s$ is the isentropic efficiency. (Fu & Gundersen 2012; Raiko 2013, p. 2-3; Raiko & Saarenpää 2014, p. 10)

The compression process can be made more effective by improving the compressor efficiency, reducing the compression ratio, lowering the temperature before the compressor and decreasing the mass flow. (Fu & Gundersen 2012)

# 5. OXYGEN SEPARATION PROCESS SIMULATION WITH ASPEN PLUS

The software used for the simulation is a steady-state simulator AspenPlus using Peng-Robinson physical property method. The Peng-Robinson equation is defined as:

$$p = \frac{R_u T}{V_m - b} - \frac{a\propto}{V_m(V_m+b)+b(V_m-b)} \tag{5.1}$$

where $p$ is pressure, $R_u$ is the ideal gas constant, $T$ is temperature, $V_m$ is the molar volume and the coefficients $a$ and $b$ and the dimensionless constant $\alpha$ are

$$a = \frac{0.457235 R_u^2 T_c^2}{p_c} \tag{5.2}$$

$$b = \frac{0.077796 \mathrm{R}_u T_c}{p_c} \tag{5.3}$$

$$\propto = \left(1 + \kappa(1 - T_r^{0.5})\right)^2 \tag{5.4}$$

where $T_c$ and $p_c$ are temperature and pressure at the critical point respectively and $\kappa$ is

$$\kappa = 0.37464 + 1.54226\omega - 0.26692\omega^2 \tag{5.5}$$

where $\omega$ is the acentric factor and reduced temperature $T_r$ is

$$T_r = \frac{T}{T_c} \tag{5.6}$$

(Peng & Robinson 1976).

The components included in the simulation are $O_2$, $N_2$ and Ar. An air separation template with metric units is used to preset some of the calculation preferences. (AspenPlus 2014)

## 5.1 Description of the simulation model

The simplest process option of the Nurmia oxygen enrichment process is chosen for the simulation in order to achieve a functioning model with a possibility for sensitivity analysis. Two different simulation cases are carried out. The first simulation case is configured for medium purity oxygen product and the second one is configured to produce

high purity oxygen product. The simulation models are identical, except for the operation specifications in the low pressure column.

A flowsheet model of the simplest Nurmia oxygen enrichment process is assembled with the flowsheeting tool of the software. Calculation blocks FSplit, Mixer, Compr, MHeatX, HeatX, Valve and RadFrac are used to create the simulation model. Their functionalities are presented in Table 4.

***Table 4.*** *Equipment representing the process flowsheet symbols.*

| **Block names** | **ASPEN model** | **Functionality** |
|---|---|---|
| SEP | FSplit | Separator |
| MIX | Mixer | Mixer |
| COMP1- COMP2 | Compr | Compressor |
| HEX1 | MHeatX | Heat exchanger, countercurrent, multipassage |
| HEX2-HEX5 | HeatX | Heat exchanger, countercurrent |
| THR | Valve | Throttle |
| HP | RadFrac | High pressure column, condenser |
| LP | RadFrac | Low pressure column, evaporator |

The simulation model is created in order to study process parameters, required external energy, internal heat streams and process yield with chosen input parameters. The simulation model illustrates an equilibrium state of the process. The model illustrates a theoretical and simplified version of the Nurmia oxygen enrichment process. A commercial process would be more complex with columns with several stages and possibly a reflux circulation of remaining process medium to achieve better efficiency and higher yield.

In the first simulation case, the low pressure column has a distillate rate of 2 kmol/h as the operating specification. The second case is otherwise identical, but the oxygen concentrate rate from the low pressure column is adjusted to be 1 kmol/h.

Separator SEP has been configured to divide the air flow between the heat exchangers with a fraction of 0.8 to HEX1 and 0.2 to HEX2 in simulation Case 1 and 0.9 to HEX1 and 0.1 to HEX2 in simulation Case 2. The distillation column blocks operate using both vapor and liquid as vapor phases and a cryogenic convergence setting. The high pressure column HP is configured to be a vapor-liquid-condenser with 16 theoretical stages and with a pressure level of 1 bar and a bottoms rate of 4 kmol/h as an operating specification. The low pressure column is a kettle-type evaporator with 11 theoretical stages with a pressure level of 0.7 bar in the first section and 0.18 bar in the second. All

of the heat produced in the HP is distributed into the LP. The compressors COMP1 and COMP2 are simulated using isentropic compressor blocks and the compressor efficiency is 0.72.

The model flowsheet shown in Figure 16 starts with input air. The air is presumed to be pretreated and contain no humidity, carbon dioxide or other impurities. The air is divided to two parts, which are led through the heat exchangers HEX1 and HEX2 to cool the air down. Then the two air streams are brought together in a mixer (MIX) and further cooled down to the temperature of 81.5 K in the heat exchangers HEX3, HEX4 and HEX5. A default value of heat transfer coefficient 850 W/(K $m^2$) is used in simulation for the heat exchangers, which is an estimation based on typical heat transfer coefficient values in heat exchangers. The cold input air is fed to the high pressure column (HP), where some of the oxygen condenses forming liquid oxygen concentrate.

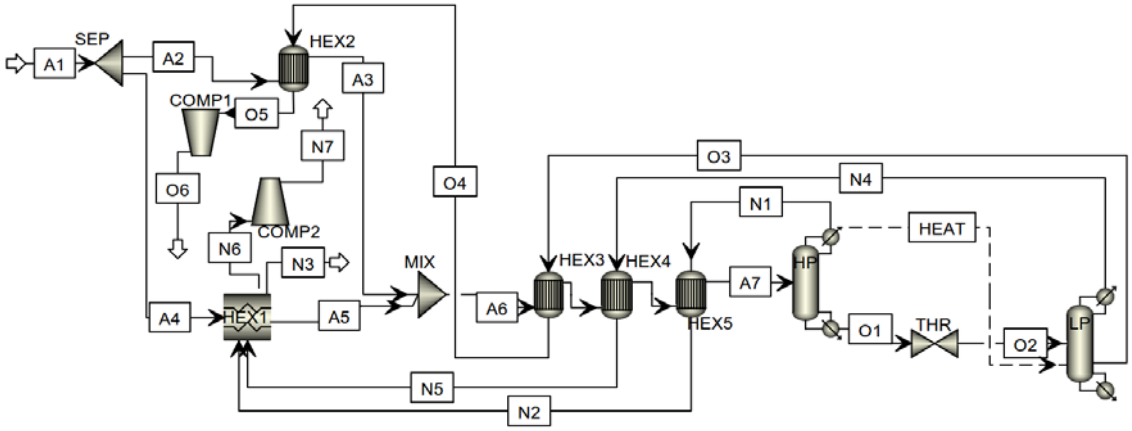


***Figure 16.*** *Flowsheet of the simulation model. Dashed line is the heat stream from the first column to the other and solid line is the material stream.*

The liquid oxygen concentrate is throttled to the pressure level of the vaporizing column (LP) and fed to it. The remaining fraction of air, which consists mostly of nitrogen, is led out of the HP column in gaseous form and out of the process through the heat exchanger arrangement. The oxygen concentrate vaporizes inside the LP column while consuming heat from the HP column. The heat stream from the first column to the second one is also included in the flowsheet. The vaporized oxygen concentrate and a separated nitrogen rich fraction are led out of the LP column, through the heat exchanger arrangement and finally compressed back to atmospheric pressure.

## 5.2 Results of the simulation

**SIMULATION CASE 1: MEDIUM PURITY OXYGEN PRODUCT**

The composition and state of air stream at different part of the process is presented in Table 5 for an input air molar flow of 10 kmol/h, which is equivalent to a mass flow of

289.7 kg/h. The input air A1 is at 293 K and 1 bar and with mole fractions of 0.78 of $N_2$, 0.21 of $O_2$ and 0.01 of Ar. The air is gradually cooled down in consecutive heat exchangers to the temperature of 84.3 K, 83.6 K, 83.7 K and finally 81.5 K. The vapor fraction, enthalpy, molar flow per component, volume flow, vapor standard volume, compressibility and isentropic constant are also given in Table 5 for each stage of the process for the input air.

***Table 5.*** *Temperature, vapor fraction, composition profiles and flowrates for input air.*

| | **A1** | **A2** | **A3** | **A4** | **A5** | **A6** | **A7** |
|---|---|---|---|---|---|---|---|
| **Temperature [K]** | 293 | 293 | 84.3 | 293 | 83.6 | 83.7 | 81.5 |
| **Pressure [bar]** | 1 | 1 | 1 | 1 | 1 | 1 | 1 |
| **Vapor Fraction** | 1 | 1 | 1 | 1 | 1 | 1 | 1 |
| **Molar Flow [kmol/h]** | 10 | 2 | 2 | 8 | 8 | 10 | 10 |
| **Mass Flow [kg/h]** | 289.697 | 57.939 | 57.939 | 231.758 | 231.758 | 289.697 | 289.697 |
| **Enthalpy [W]** | -427.114 | -85.423 | -3477.94 | -341.691 | -13965.0 | -17442.9 | -17626.2 |
| **Molar Flow [kmol/h]** | | | | | | | |
| **$N_2$** | 7.8 | 1.56 | 1.56 | 6.24 | 6.24 | 7.8 | 7.8 |
| **$O_2$** | 2.1 | 0.42 | 0.42 | 1.68 | 1.68 | 2.1 | 2.1 |
| **Ar** | 0.1 | 0.02 | 0.02 | 0.08 | 0.08 | 0.1 | 0.1 |
| **Mole Fraction** | | | | | | | |
| **$N_2$** | 0.78 | 0.78 | 0.78 | 0.78 | 0.78 | 0.78 | 0.78 |
| **$O_2$** | 0.21 | 0.21 | 0.21 | 0.21 | 0.21 | 0.21 | 0.21 |
| **Ar** | 0.01 | 0.01 | 0.01 | 0.01 | 0.01 | 0.01 | 0.01 |
| ***Vapor Phase*** | | | | | | | |
| **Volume Flow [$m^3$/h]** | 243.589 | 48.718 | 13.585 | 194.872 | 53.782 | 67.368 | 65.441 |
| **Vapor Standard Volume at 0 °C** | 224.136 | 44.827 | 44.827 | 179.309 | 179.309 | 224.136 | 224.136 |
| **Compressibility** | 0.999 | 0.999 | 0.967 | 0.999 | 0.966 | 0.966 | 0.964 |
| **Isentropic constant** | 1.403 | 1.403 | 1.442 | 1.403 | 1.443 | 1.443 | 1.446 |

The composition and state of the oxygen product at different parts of the process is listed below in Table 6. As the cold air enters the HP column, 4 kmol/h of liquid oxygen concentrate O1 condenses. The oxygen concentrate O1 has mole fractions of 0.48 of $N_2$, 0.51 of $O_2$ and 0.02 of Ar and is at 81.4 K. The O1 is then throttled to 0.7 bar and led to the second column, where it evaporates, further enriches with oxygen and is again throttled to a lower pressure of 0.18 bar to ensure compete evaporation. The resulting product O3 has mole fractions of 0.15 of $N_2$, 0.82 of $O_2$ and 0.023 of Ar and a total molar flow of 2 kmol/h, which is equivalent to a mass flow of 63.2 kg/h. After the heat exchanger arrangement and the compression to atmospheric pressure, the temperature of the oxygen product is increased to 538.7 K. The vapor fraction, enthalpy, molar flow per component and for vapor phase also volume flow, vapor standard volume, compressibility and isentropic constant are given in Table 6 for each stage of the process.

The compressor net work required for compressor COMP1 is 4119 W for compressing 63.2 kg/h oxygen concentrate from 0.18 bar to 1 bar, when the compressor efficiency is 0.72.

***Table 6.*** *Temperature, vapor fraction, composition profiles and flowrates for oxygen concentrate.*

| | **O1** | **O2** | **O3** | **O4** | **O5** | **O6** |
|---|---|---|---|---|---|---|
| **Temperature [K]** | 81.4 | 78.4 | 74.9 | 80.1 | 290.8 | 538.7 |
| **Pressure [bar]** | 1 | 0.7 | 0.18 | 0.18 | 0.18 | 1 |
| **Vapor Fraction** | 0 | 0.027 | 1 | 1 | 1 | 1 |
| **Molar Flow [kmol/h]** | 4 | 4 | 2 | 2 | 2 | 2 |
| **Mass Flow [kg/h]** | 120.906 | 120.906 | 63.15 | 63.15 | 63.15 | 63.15 |
| **Enthalpy [W]** | -13952.8 | -13952.8 | -3593.16 | -3509.8 | -117.279 | 4002.076 |
| **Molar Flow [kmol/h]** | | | | | | |
| **$N_2$** | 1.91 | 1.91 | 0.305 | 0.305 | 0.305 | 0.305 |
| **$O_2$** | 2.025 | 2.025 | 1.648 | 1.648 | 1.648 | 1.648 |
| **Ar** | 0.066 | 0.066 | 0.047 | 0.047 | 0.047 | 0.047 |
| **Mole Fraction** | | | | | | |
| **$N_2$** | 0.477 | 0.477 | 0.153 | 0.153 | 0.153 | 0.153 |
| **$O_2$** | 0.506 | 0.506 | 0.824 | 0.824 | 0.824 | 0.824 |
| **Ar** | 0.016 | 0.016 | 0.023 | 0.023 | 0.023 | 0.023 |
| ***Vapor Phase*** | | | | | | |
| **Volume Flow [$m^3$/h]** | | 0.994 | 68.809 | 73.623 | 268.729 | 89.618 |
| **Vapor Standard Volume at 0 °C [$m^3$/h]** | | 2.456 | 44.825 | 44.825 | 44.825 | 44.825 |
| **Compressibility** | | 0.972 | 0.992 | 0.993 | 1 | 1 |
| **Isentropic constant** | | 1.435 | 1.413 | 1.412 | 1.401 | 1.368 |

The fraction of air that remains after the oxygen concentrate has been separated is enriched with nitrogen. Hence it is later addressed as nitrogen concentrate. The nitrogen concentrate N1 leaving the HP column at a pressure of 1 bar has a composition of 0.98 of $N_2$, 0.013 of $O_2$ and 0.006 of Ar and a molar flow of 6 kmol/h, which is equivalent to a mass flow of 168.8 kg/h. The nitrogen concentrate N4 leaving the LP column at a pressure of 0.7 bar has a mole fractions of 0.80 of $N_2$, 0.19 of $O_2$ and 0.009 of Ar and a molar flow of 2 kmol/h, which is equivalent to a mass flow of 57.8 kg/h. The temperature, vapor fraction, enthalpy, molar flow per component and for vapor phase also volume flow, vapor standard volume, compressibility and isentropic constant are also given in Table 7 for each stage of the process.

The compressor net work for compressor COMP2 is 695 W for compressing 57.8 kg/h nitrogen concentrate when the compressor efficiency is 0.72. The compression increases the pressure from 0.7 bar to 1 bar.

***Table 7.*** *Temperature, vapor fraction, composition profiles and flowrates for nitrogen concentrate.*

| | N1 | N2 | N3 | N4 | N5 | N6 | N7 |
|---|---|---|---|---|---|---|---|
| **Temperature** | 77.6 | 79.2 | 288.4 | 78.1 | 79.1 | 288.4 | 331.7 |
| **Pressure [bar]** | 1 | 1 | 1 | 0.7 | 0.7 | 0.7 | 1 |
| **Vapor Fraction** | 1 | 1 | 1 | 1 | 1 | 1 | 1 |
| **Molar Flow [kmol/h]** | 6 | 6 | 6 | 2 | 2 | 2 | 2 |
| **Mass Flow [kg/h]** | 168.791 | 168.791 | 168.791 | 57.753 | 57.753 | 57.753 | 57.753 |
| **Enthalpy [W]** | -10781.8 | -10698.5 | -472.106 | -3571.08 | -3554.42 | -156.493 | 538.646 |
| **Molar Flow [kmol/h]** | | | | | | | |
| **$N_2$** | 5.89 | 5.89 | 5.89 | 1.605 | 1.605 | 1.605 | 1.605 |
| **$O_2$** | 0.075 | 0.075 | 0.075 | 0.376 | 0.376 | 0.376 | 0.376 |
| **Ar** | 0.034 | 0.034 | 0.034 | 0.019 | 0.019 | 0.019 | 0.019 |
| **Mole Fraction** | | | | | | | |
| **$N_2$** | 0.982 | 0.982 | 0.982 | 0.802 | 0.802 | 0.802 | 0.802 |
| **$O_2$** | 0.013 | 0.013 | 0.013 | 0.188 | 0.188 | 0.188 | 0.188 |
| **Ar** | 0.006 | 0.006 | 0.006 | 0.009 | 0.009 | 0.009 | 0.009 |
| ***Vapor Phase*** | | | | | | | |
| **Volume Flow [$m^3$/h]** | 37.222 | 38.098 | 143.928 | 18.081 | 18.33 | 68.544 | 55.14 |
| **Vapor Standard Volume at 0 °C [$m^3$/h]** | 134.482 | 134.482 | 134.482 | 44.827 | 44.827 | 44.827 | 44.827 |
| **Compressibility** | 0.96 | 0.962 | 0.999 | 0.972 | 0.973 | 1 | 1 |
| **Isentropic constant** | 1.45 | 1.448 | 1.403 | 1.435 | 1.434 | 1.403 | 1.401 |

In the simulation model, the input air is cooled down in five separate heat exchangers. This is to achieve better efficiency by dividing the cooling down of the input air into several stages and thus minimizing exergy losses in the heat transfer process. The smaller the temperature difference between the hot and the cold flow, the smaller the exergy loss there is in a heat exchanger.

A default value of heat transfer coefficient 850 W/(K $m^2$) is used in simulation for the heat exchangers. With a total input air flow of 10 kmol/h in the heat exchangers there is a total of 17.2 kW heat transferred. This is divided between the HEX1 as 13.6 kW, HEX2 3.4 kW, HEX3 as 0.08 kW, HEX4 as 0.02 kW and HEX5 as 0.08 kW. Thus the total size of heat transfer surface would be 4.9 $m^2$, when the heat transfer coefficient is 850 W/(K $m^2$). Heat transfer surface per heat exchanger would be 3.6 $m^2$ for HEX1, 1.28 $m^2$ for HEX2, 0.020 $m^2$ for HEX3, 0.0050 $m^2$ for HEX4 and 0.023 $m^2$ for HEX5. The heat exchanger characteristics are listed in Table 8.

***Table 8.*** *Heat exchanger duty and heat transfer area in the simulation model.*

| | HEX1 | HEX2 | HEX3 | HEX4 | HEX5 | SUM |
|---|---|---|---|---|---|---|
| **Type** | Counter-current, multi-passage | Counter-current | Counter-current | Counter-current | Counter-current | - |
| **U [W/(Km$^2$)]** | 850 | 850 | 850 | 850 | 850 | - |
| **Heat transferred [kW]** | 13.623 | 3.393 | 0.083 | 0.017 | 0.083 | 17.199 |
| **Heat transfer surface area [m$^2$]** | 3.57924 | 1.2837 | 0.02046 | 0.004961 | 0.02366 | 4.9120 |

Heat transfer between the two columns is 7101 W. The evaporation consumes 6786 W and the condensation releases 7101 W.

## SIMULATION CASE 2: HIGH PURITY OXYGEN PRODUCT

High purity simulation case is otherwise identical to the medium purity case, except that the low pressure column configurations are different as described before. This causes changes in the simulation results. In Table 9 are the temperatures, vapor fractions, composition profiles and flow rates of input air, which are largely similar to the results in Case 1.

***Table 9.*** *Temperature, vapor fraction, composition profiles and flowrates for input air.*

| | A1 | A2 | A3 | A4 | A5 | A6 | A7 |
|---|---|---|---|---|---|---|---|
| **Temperature [K]** | 293 | 293 | 81.3 | 293 | 83 | 82.6 | 81.4 |
| **Pressure [bar]** | 1 | 1 | 1 | 1 | 1 | 1 | 1 |
| **Vapor Fraction** | 1 | 1 | 0.986 | 1 | 1 | 1 | 1 |
| **Molar Flow [kmol/h]** | 10 | 1 | 1 | 9 | 9 | 10 | 10 |
| **Mass Flow [kg/h]** | 289.697 | 28.97 | 28.97 | 260.72 | 260.7 | 289.6 | 289.697 |
| **Enthalpy [W]** | -427.11 | -42.711 | -1787.5 | -384.40 | -15752 | -17539 | -17634 |
| **Molar Flow [kmol/h]** | | | | | | | |
| **$N_2$** | 7.8 | 0.78 | 0.78 | 7.02 | 7.02 | 7.8 | 7.8 |
| **$O_2$** | 2.1 | 0.21 | 0.21 | 1.89 | 1.89 | 2.1 | 2.1 |
| **Ar** | 0.1 | 0.01 | 0.01 | 0.09 | 0.09 | 0.1 | 0.1 |
| **Mole Fraction** | | | | | | | |
| **$N_2$** | 0.78 | 0.78 | 0.78 | 0.78 | 0.78 | 0.78 | 0.78 |
| **$O_2$** | 0.21 | 0.21 | 0.21 | 0.21 | 0.21 | 0.21 | 0.21 |
| **Ar** | 0.01 | 0.01 | 0.01 | 0.01 | 0.01 | 0.01 | 0.01 |
| ***Vapor Phase*** | | | | | | | |
| **Volume Flow [m$^3$/h]** | 243.589 | 24.359 | 6.441 | 219.231 | 60.072 | 66.354 | 65.358 |
| **Vapor Standard Volume at 0 °C** | 224.136 | 22.414 | 22.107 | 201.723 | 201.723 | 224.136 | 224.136 |
| **Compressibility** | 0.999 | 0.999 | 0.964 | 0.999 | 0.965 | 0.965 | 0.964 |
| **Isentropic constant** | 1.403 | 1.403 | 1.446 | 1.403 | 1.444 | 1.444 | 1.446 |

In Table 10 are the simulation results regarding oxygen concentrate streams. The most important difference to Case 1 results are the smaller molar flow of oxygen concentrate product and the higher oxygen content of it. The compressor net work required for compressor COMP1 is 2062 W for compressing 32.0 kg/h oxygen concentrate from 0.18 bar to 1 bar when the compressor efficiency is 0.72.

***Table 10.*** *Temperature, vapor fraction, composition profiles and flowrates for oxygen concentrate.*

| | **O1** | **O2** | **O3** | **O4** | **O5** | **O6** |
|---|---|---|---|---|---|---|
| **Temperature [K]** | 81.4 | 78.4 | 75.9 | 76.3 | 292 | 537.8 |
| **Pressure [bar]** | 1 | 0.7 | 0.18 | 0.18 | 0.18 | 1 |
| **Vapor Fraction** | 0 | 0.027 | 1 | 1 | 1 | 1 |
| **Molar Flow [kmol/h]** | 4 | 4 | 0.999 | 0.999 | 0.999 | 0.999 |
| **Mass Flow [kg/h]** | 120.906 | 120.906 | 32.002 | 32.002 | 32.002 | 32.002 |
| **Enthalpy [W]** | -13953 | -13953 | -1797.1 | -1794.1 | -49.264 | 2012.337 |
| **Molar Flow [kmol/h]** | | | | | | |
| **$N_2$** | 1.91 | 1.91 | trace | trace | trace | trace |
| **$O_2$** | 2.025 | 2.025 | 0.995 | 0.995 | 0.995 | 0.995 |
| **Ar** | 0.066 | 0.066 | 0.004 | 0.004 | 0.004 | 0.004 |
| **Mole Fraction** | | | | | | |
| **$N_2$** | 0.477 | 0.477 | 6 PPM | 6 PPM | 6 PPM | 6 PPM |
| **$O_2$** | 0.506 | 0.506 | 0.996 | 0.996 | 0.996 | 0.996 |
| **Ar** | 0.016 | 0.016 | 0.004 | 0.004 | 0.004 | 0.004 |
| ***Vapor Phase*** | | | | | | |
| **Volume Flow [$m^3$/h]** | | 0.994 | 34.821 | 34.996 | 134.787 | 44.684 |
| **Vapor Standard Volume at 0 °C [$m^3$/h]** | | 2.456 | 22.391 | 22.391 | 22.391 | 22.391 |
| **Compressibility** | | 0.972 | 0.992 | 0.992 | 1 | 1 |
| **Isentropic constant** | | 1.435 | 1.41 | 1.41 | 1.397 | 1.361 |

In Table 11 are the properties of nitrogen concentrate streams in the simulated process. The main difference to the results of Case 1 is that the flow rate of nitrogen concentrate from the low pressure column is higher and its oxygen content higher. This is because a larger fraction of the total process stream is separated from the oxygen concentrate when producing oxygen concentrate with a higher purity. The compressor net work for compressor COMP2 is 1048 W for compressing 88.90 kg/h nitrogen concentrate from 0.7 bar to 1 bar, when the compressor efficiency is 0.72.

***Table 11.*** *Temperature, vapor fraction, composition profiles and flowrates for nitrogen concentrate.*

| | N1 | N2 | N3 | N4 | N5 | N6 | N7 |
|---|---|---|---|---|---|---|---|
| **Temperature [K]** | 77.6 | 79.2 | 289.9 | 80.5 | 80.8 | 289.9 | 333.2 |
| **Pressure [bar]** | 1 | 1 | 1 | 0.7 | 0.7 | 0.7 | 1 |
| **Vapor Fraction** | 1 | 1 | 1 | 1 | 1 | 1 | 1 |
| **Molar Flow [kmol/h]** | 6 | 6 | 6 | 3.001 | 3.001 | 3.001 | 3.001 |
| **Mass Flow [kg/h]** | 168.791 | 168.791 | 168.791 | 88.903 | 88.903 | 88.903 | 88.903 |
| **Enthalpy [W]** | -10782 | -10698 | -406.92 | -5285.8 | -5277.4 | -201.51 | 846.479 |
| **Molar Flow [kmol/h]** | | | | | | | |
| **$N_2$** | 5.89 | 5.89 | 5.89 | 1.91 | 1.91 | 1.91 | 1.91 |
| **$O_2$** | 0.075 | 0.075 | 0.075 | 1.09 | 1.09 | 1.09 | 1.09 |
| **Ar** | 0.034 | 0.034 | 0.034 | 0.061 | 0.061 | 0.061 | 0.061 |
| **Mole Fraction** | | | | | | | |
| **$N_2$** | 0.982 | 0.982 | 0.982 | 0.636 | 0.636 | 0.636 | 0.636 |
| **$O_2$** | 0.013 | 0.013 | 0.013 | 0.343 | 0.343 | 0.343 | 0.343 |
| **Ar** | 0.006 | 0.006 | 0.006 | 0.02 | 0.02 | 0.02 | 0.02 |
| ***Vapor Phase*** | | | | | | | |
| **Volume Flow [$m^3$/h]** | 37.222 | 38.099 | 144.61 | 27.977 | 28.102 | 103.329 | 83.139 |
| **Vapor Standard Volume at 0 °C [$m^3$/h]** | 134.482 | 134.482 | 134.482 | 67.262 | 67.262 | 67.262 | 67.262 |
| **Compressibility** | 0.96 | 0.962 | 0.999 | 0.974 | 0.974 | 1 | 1 |
| **Isentropic constant** | 1.45 | 1.448 | 1.403 | 1.435 | 1.434 | 1.404 | 1.402 |

With a total input air flow of 10 kmol/h in the heat exchangers there is a total of 17.2 kW heat transferred, which is the same as in Case 1. This is divided between the HEX1 as 15.37 kW, HEX2 1.75 kW, HEX3 as 0.08 kW, HEX4 as 0.007 kW and HEX5 as 0.003 kW. Thus the total size of heat transfer surface would be 7.06 $m^2$, when the heat transfer coefficient is 850 W/(K $m^2$). The heat exchanger characteristics are listed in Table 12.

***Table 12.*** *Heat exchanger duty and heat transfer area in the simulation model.*

| | HEX1 | HEX2 | HEX3 | HEX4 | HEX5 | SUM |
|---|---|---|---|---|---|---|
| **Type** | Counter-current, multipas-sage | Counter-current | Counter-current | Counter-current | Counter-current | - |
| **U [W/(Km$^2$)]** | 850 | 850 | 850 | 850 | 850 | - |
| **Heat transferred [kW]** | 15.367 | 1.745 | 0.083 | 0.007 | 0.003 | 17.205 |
| **Heat transfer surface area [m$^2$]** | 5.6820 | 1.3551 | 0.02705 | 0.000102 | 0.000671 | 7.0650 |

Heat transfer between the high pressure and the low pressure column is 7100 W, when the evaporation consumes 7100 W and the condensation releases 7140 W.

## 5.3 Sensitivity analysis

A sensitivity analysis is carried out for the simulation model in order to investigate the relationships between input and output variables and to test and verify the functionality of the model.

The degrees of freedom for the Nurmia oxygen enrichment process are the flow rate of input air and the liquefaction fraction, which is defined by the pressure in the first section of the low pressure column. A sensitivity analysis using the input air flow rate and the pressure in the first section of the low pressure column is performed below. Also an investigation regarding the effect of intermediate cooling during compression of the oxygen concentrate is carried out.

Varying the input air molar flow to the process has an effect on the compressor work needed in the process. The compressor duties needed to compress the oxygen and nitrogen concentrates separated in the process with the product oxygen content of 82 mol-% are plotted in Figure 17.

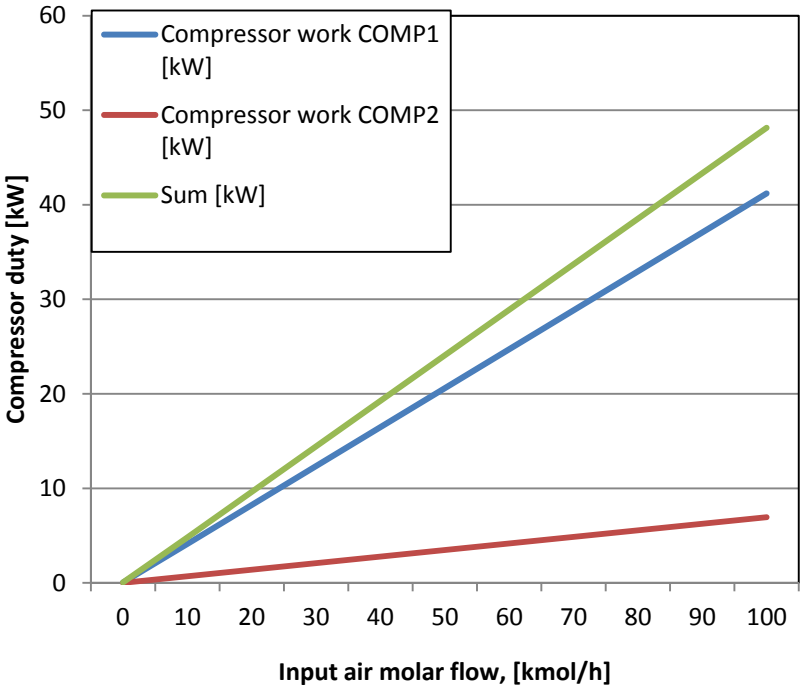


***Figure 17.*** *Compressor duties of compressors COMP1 and COMP2 as a function of input molar flow of air.*

Compressor COMP1 is for the oxygen concentrate with a purity of 82 mol-% and COMP2 is for the nitrogen concentrate. The compressor duty reaches values 41.1 kW for COMP1 and 6.9 kW for COMP2, when the input air molar flow is increased to 100 kmol/h. The duty to both compressors increases linearly when the input air flow is increased. The increase is perfectly linear because the simulation model is more ideal than a real process. In a real process total losses of the process would relatively decrease if the input flow was increased. This would lead to a decreasing slope of the compressor duty plot.

The effect of varying the mass flow of oxygen concentrate and the concentration of oxygen in the product to the compressor power for COMP1 is presented in Figure 18. The efficiency of the compressor in this example is 0.8.

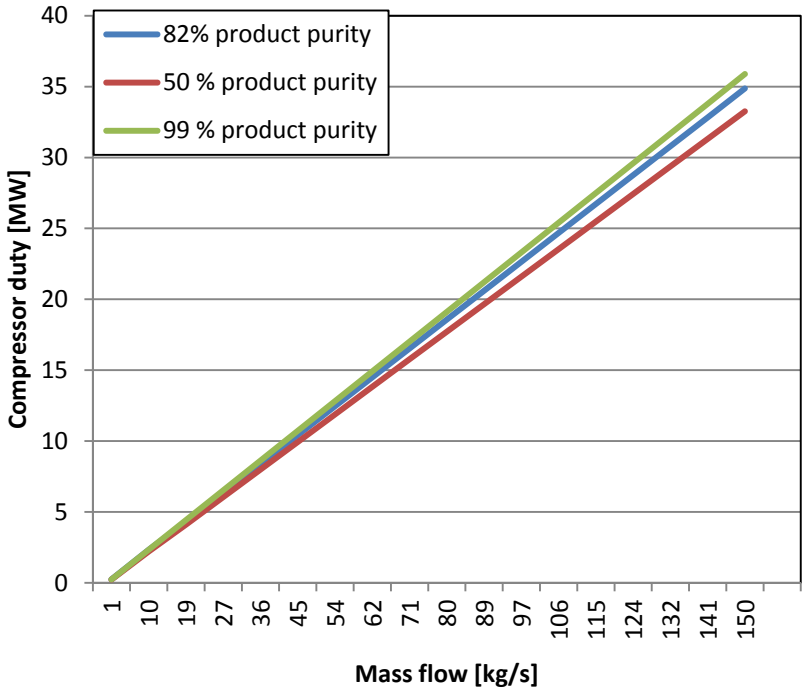


***Figure 18.*** *The compressor duty to compressing oxygen concentrate with oxygen molar fractions of 0.82 and 0.5 from 0.18 bar to 1 bar, when the compressor efficiency is 0.8.*

The compression work increases linearly with the mass flow for all three product purities during the range of mass flow examined. The power needed for compression is slightly higher for the mixture with higher oxygen content. The compression work depends on the enthalpy difference over the compressor as seen in equation (4.29). The compressor duty is calculated using the temperature and pressure values acquired from the simulation results. This is due to the larger enthalpy change over the compressor for the concentrate with higher oxygen content. Thus the compression work is higher for the concentrate with higher oxygen content.

The effect of varying the mass flow of nitrogen concentrate from simulation Case 1 to the compressor power for COMP2 is presented in Figure 19. The equation (4.29) with properties listed in Chapter 3 can be used to evaluate the compression energy of nitrogen concentrate and by using temperature and pressure levels acquired from the simulation results. The efficiency of the compressor in this example is 0.8.

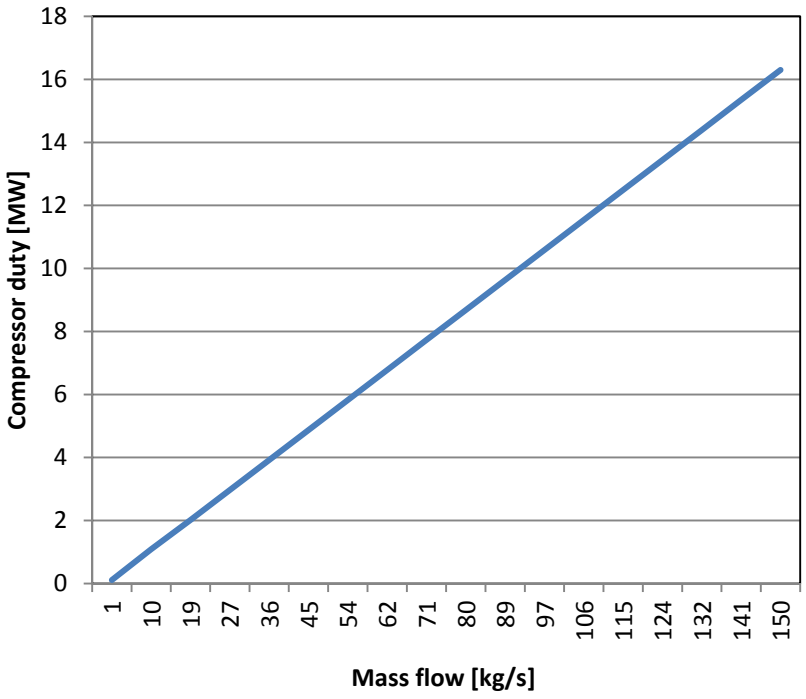


***Figure 19.*** *The compressor duty to compressing nitrogen concentrate from 0.4 bar to 1 bar, with compressor efficiency of 0.8.*

The compressor duty to compressing nitrogen concentrate presented in Figure 19 is lower than the compressor duty to compressing oxygen concentrate presented in Figure 18. This is because the oxygen concentrate in this simulation model is compressed from 0.18 bar to 1 bar and the nitrogen concentrate is only compressed from 0.4 bar to 1 bar.

The effects of varying the pressure of the first section of low pressure column with simulation Case 1 configuration to the compressor duty of COMP1 while keeping the other process variables constant are illustrated in Figure 20. The pressure level at the second section of the low pressure column is kept constant at 0.18 bar.

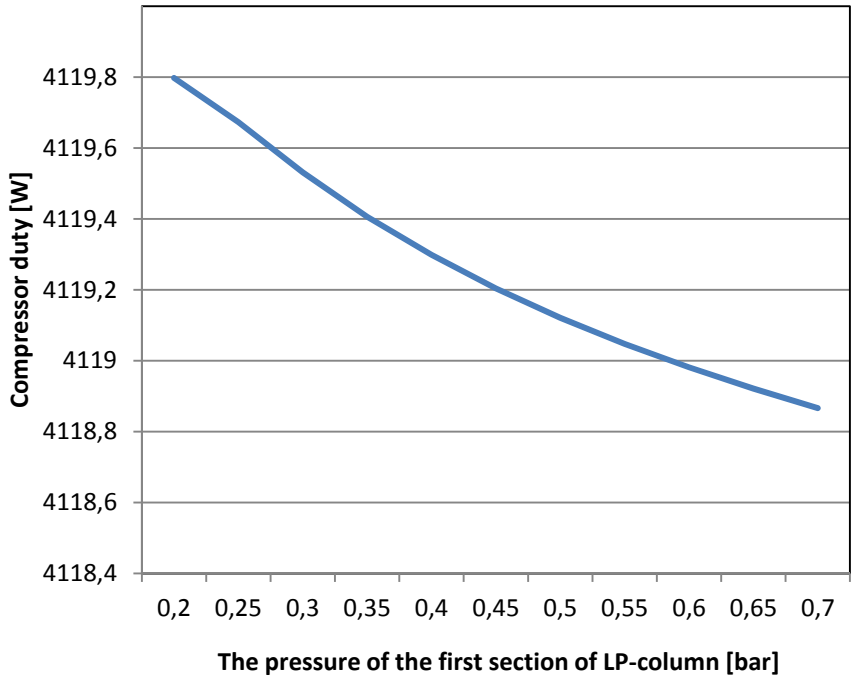


***Figure 20.*** *Compressor duty to compressor COMP1 as a function of the pressure in the first section of the low pressure column.*

Compressor COMP1 is used for compressing the gaseous oxygen concentrate product in the simulated process. Compressor power can be altered by changing either the compression ratio, the temperature before the compressor or the mass flow.

The compressor duty to compressing the oxygen concentrate product slightly decreases when the pressure of the first section of the low pressure column increases. One reason for this can be that the mass flow of the oxygen product decreases when the liquid is not evaporated until the lower part of the column. Consequently, a larger fraction of oxygen is exiting the process in the nitrogen rich waste stream.

The pressure in the first section of the evaporation column also influences the fraction of that flow that is liquefied. Lowering the pressure increases the amount of liquid oxygen concentrate that is liquefied in the high pressure column, and therefore also increases the mass flow of the compressor.

The effects of varying the pressure of the first section of low pressure column with simulation Case 1 configuration to the compressor duty COMP2 is illustrated in Figure 21. Other process variables are kept constant as defined before.

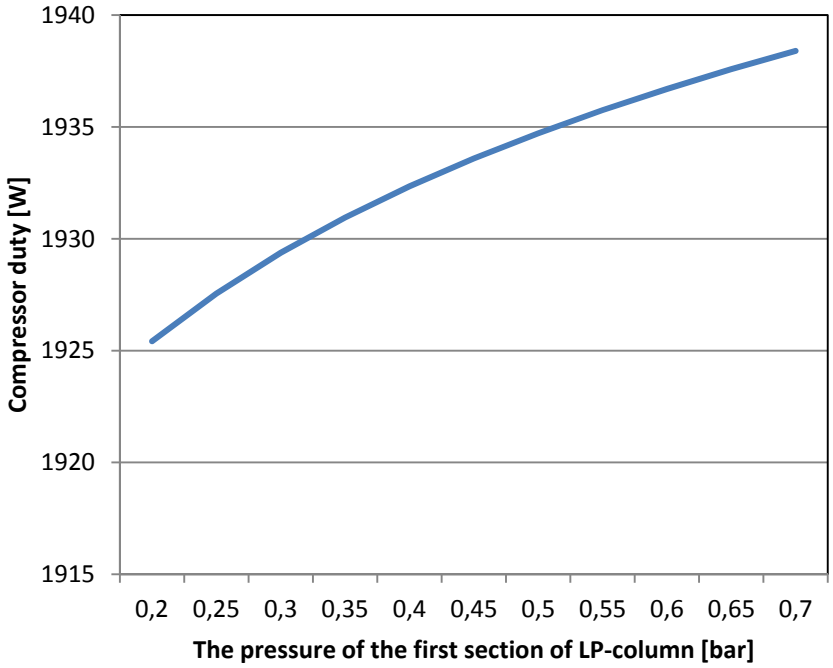


***Figure 21.*** *Compressor duty for compressor COMP2 as a function of the pressure of the first section of the low pressure column.*

In the simulation model the compressor COMP2 is used to compress the waste flow of the process consisting mainly of nitrogen, later on addressed as nitrogen concentrate. The compressor duty to compressing nitrogen concentrate increases when the pressure at the first section of the low pressure is increased. This can be due to the increasing mass flow of nitrogen concentrate, because a larger fraction of the process air is left behind when the liquefaction fraction decreases.

Other reason for the increasing compressor duty can be that the mass flow of nitrogen concentrate also increases, because the liquid input only vaporizes in the second stage of the column. The mass flow of oxygen product decreases, when the liquid is not evaporated until in the lower part of the column. Consequently, a larger fraction of oxygen is exiting the process in the nitrogen rich waste stream.

The effects of varying the pressure of the first section of low pressure column with simulation Case 1 configurations to the mole fraction of oxygen in the oxygen concentrate product is presented in Figure 22. The pressure of the first section on the low pressure column controls the fraction of air that is liquefied in the high pressure column and the rate on evaporation in the low pressure column.

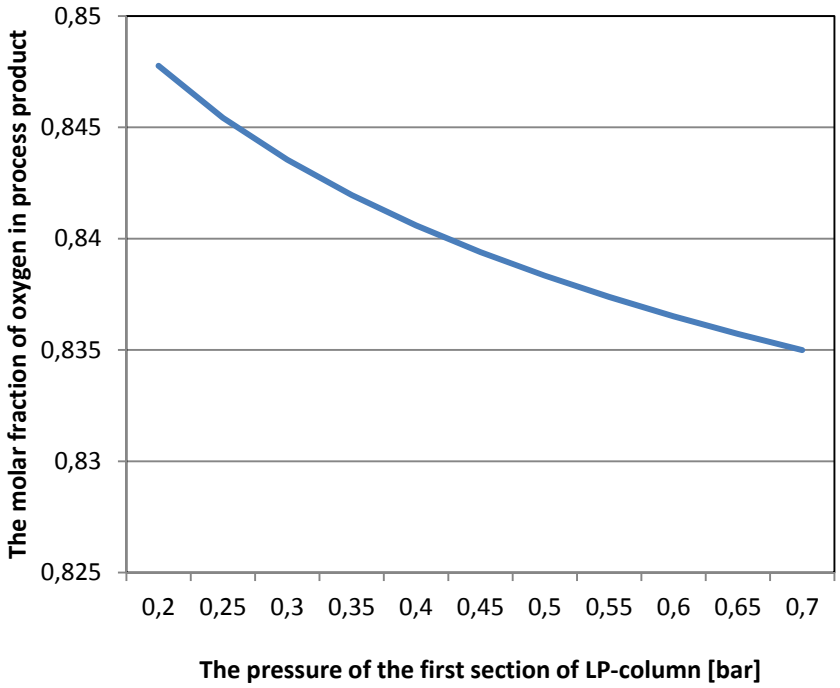


***Figure 22.*** *The molar fraction of oxygen in the final process product as a function of the pressure of the first section of the low pressure column.*

The purity of the process product in the simulation model is affected by the number of equilibrium sections called theoretical plates and the enrichment factor during separation controlled by pressure. The oxygen fraction in the product decreases slightly when the pressure of the first section of the low pressure column is increased. This can be caused by the decrease in the enrichment factor. The lower the pressure, the higher the enrichment coefficient of oxygen there is in the equilibrium state of nitrogen and liquid oxygen.

The effect of cooling during the compression of the oxygen concentrate is investigated by exchanging the COMP1 compressor from simulation Case 1 with a multistage compressor block MCompr with cooling during both compressor stages and an isentropic efficiency of 0.72. The results of varying the amount of heat removed during the compression as a function of the compressor duty are presented in Figure 23. The reference point for compressor duty when 0 W of heat is removed comes from the original simulation model. The cooling can be carried out for example by using a water stream.

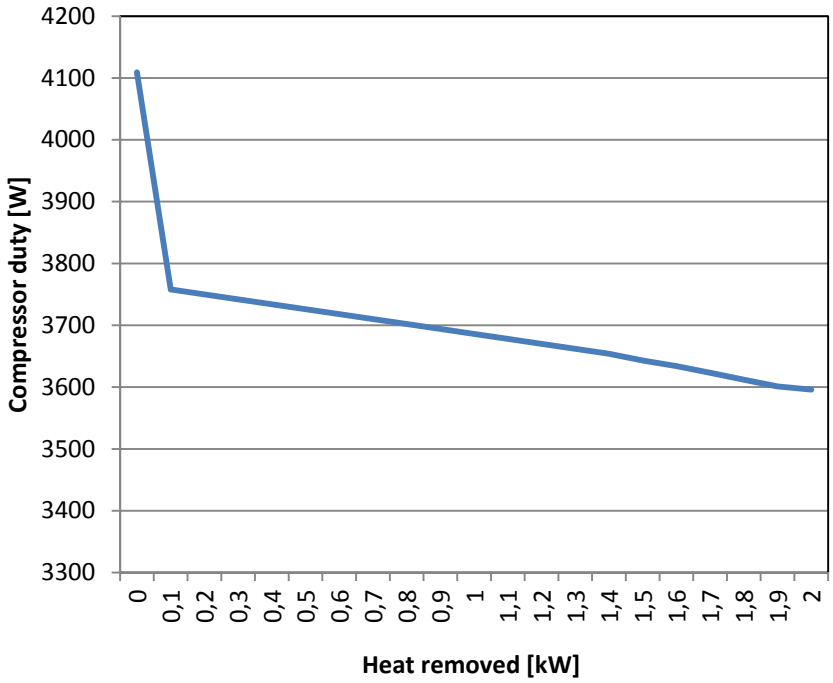


***Figure 23.*** *The effect of intermediate cooling to the compressor duty of COMP1.*

Cooling during the compression decreases the compressor work. This is caused by the decreasing enthalpy difference over the compressor as seen from equation (4.29). The rapid change in compressor duty between 0W and 0.1 kW of heat removed is caused by the transition from a regular compressor to a two-stage compressor with heat removal.

# 6. DISCUSSION

The performance characteristics of the Nurmia oxygen enrichment process and the conventional process Linde-Frankl are listed in Table 13. The Linde-Frankl process uses approximately two to three times more energy to compress a mass unit of oxygen product than the Nurmia oxygen enrichment process, depending on the Nurmia process configuration. The compression work per mass unit of oxygen is considerably less for Nurmia oxygen enrichment process than in Linde-Frankl process.

For Linde-Frankl process the compression work is 882 kJ/kg of oxygen, which is equivalent to 245 kWh/ton of the oxygen product. The compression work is 273 kJ/kg for Nurmia process with 50 mol-% purity of oxygen and 399 kJ/kg with 83 mol-% purity of oxygen, which are equivalent to 75 and 110 kWh/ton of the oxygen product. The theoretical simulation model described in Chapter 5 gives a compression work of 274.4 kJ/kg for 82 mol-% purity of oxygen, which is equivalent to 76 kWh/ton of the oxygen product. The simulation configuration producing 99.6 % purity of oxygen gives a compression work of 350 kJ/kg, which is equivalent to 97 kWh/ton of the oxygen product. The compression work could be decreased if additional intermediate cooling during compression was used, as presented in Figure 23.

Nurmia process operates at nearly atmospheric pressure, so there is less energy needed to compress the air to higher pressure level than in Linde-Frankl process. The temperature difference between the ends of the two columns is considerately lower for Nurmia process than in Linde-Frankl process due to the lower pressure level. Hence the separation process is closer to reversible ideal process and thus more efficient. Due to low pressure levels in Nurmia oxygen enrichment process, the wall structures do not need to be as strong and robust as in Linde-Frankl process.

The fraction of the total flow of gas that is liquefied is much smaller for Nurmia oxygen enrichment process, because only the oxygen fraction is liquefied. The exact fraction liquefied can be adjusted by changing the pressure of the first section in the low pressure column. In Nurmia oxygen enrichment process, there is less energy needed to perform the phase transitions. In Linde-Frankl process the entire input air flow is liquefied.

Temperature difference between the high and low pressure columns illustrates how close to reversibility does the process operate. For Nurmia oxygen enrichment process the temperature difference between condensation and evaporation is only 7.5 K due to the low pressure difference between condensation and evaporation. For Linde-Frankl process the temperature difference is approximately 20 K. (Nurmia 2003)

***Table 13.*** *Performance characteristics of Nurmia oxygen enrichment and Linde-Frankl process.*

| | Nurmia oxygen enrichment | Linde-Frankl |
|---|---|---|
| Compression work per mass unit of oxygen product<br><br>(Nurmia 2003) | 50 % purity of oxygen:<br>273 kJ/kg = 75 kWh/t<br><br>83 % purity of oxygen:<br>399 kJ/kg = 111 kWh/t<br><br>Simulated process:<br><br>82 % purity of oxygen:<br>274 kJ/kg = 76 kWh/t<br><br>99.6 % purity of oxygen:<br>350 kJ/kg = 97 kWh/t | 882 kJ/kg = 245 kWh/t |
| Fraction of the total flow of gas that is liquefied<br><br>$\dot{m}_l / \dot{m}$ | Variable,<br><br>0.417 in simulated process | 1 |
| Temperature difference between the high and low pressure columns<br><br>(Nurmia 2003) | 7.5 K | 20 K |
| Purity of product<br><br>mol-% | 50-99.6 mol-% depending on the process option chosen (Nurmia 2003) | Over 99.5 mol-% (Agrawal & Herron 2000) |
| Yield to feed ratio<br><br>$\dot{m}_{product}/\dot{m}_{feed}$ | Simulated process:<br><br>82 % purity of oxygen:<br>0.218<br><br>99.6 % purity of oxygen:<br>0.110 | Typical value ~0.226<br>(Agrawal & Herron 2000) |

A yield to feed ratio describes the productivity of the process. The smaller the yield to feed ratio, the larger is the fraction of the total amount of oxygen in input air that is lost among the exiting process streams. In Nurmia oxygen enrichment process, the more

nitrogen is left in the product oxygen, the less energy is required. For the simulated process presented in Chapter 5, the yield to feed ratio is 0.218 $kg_{product}/kg_{feed}$ for 82 % purity of oxygen product and 0.110 $kg_{product}/kg_{feed}$ for 99 % purity of the oxygen product. For Linde-Frankl process with a double column, the typical value is approximately 0.226 $kg_{product}/kg_{feed}$ (Agrawal & Herron 2000).

In Nurmia oxygen enrichment process (Nurmia 2003), the purity of the oxygen product varies greatly depending on the process configuration and parameters chosen. Energy saving processes can be utilized by leaving some of the oxygen in the nitrogen rich waste stream. This decreases the theoretical separation work. For a process with a single section low pressure column, the purity of product is 50 mol-%. If the number of evaporation stages in low pressure column is increased to two, the purity of product increases to up to 99 mol-%. For the process configuration used in the simulation model in Case 1, the purity of the oxygen concentrate product is 82 mol-% and for Case 2 the purity is 99 mol-%. For Linde-Frankl process, the typical product purity is 99.5 mol-% or higher (Agrawal & Herron 2000).

The simulated Nurmia oxygen enrichment process is able to produce its own refrigeration, when a heat exchanger configuration as presented is used. It requires heat exchanger surface area of 4.9 $m^2$ with a default value of heat transfer coefficient 850 W/(K $m^2$) when the input air flow is 10 kmol/h. For the simulated process producing high purity oxygen product, the corresponding heat exchanger area requirement is 7.1 $m^2$. In practice, this requires detailed heat exchanger design in order to avoid pressure and thermal losses.

The insulation of the process set-up has to be effective to keep the process adiabatic. This is due to the fact that the densities of the heat flow rates inside the set-up process are extremely small due to the small temperature differences within the process. Effectively this means that the set-up should be contained be inside a vacuum container.

The heat transfer between the two columns is 7101 W, when the evaporation consumes 6786 W and condensation releases 7101 W in the simulation producing 82 mol-% oxygen product. In the simulation producing 99 mol-% oxygen product, the heat transfer between the high pressure and the low pressure column is 7140 W, when the evaporation consumes 7100 W and the condensation releases 7140 W. The difference between the consumed and released values can be assessed to be lost by thermal losses in the system.

The performance characteristics of the simulated process listed in Table 13 are principally very consistent when compared to the values given in literature. The compression work for the simulated process producing 82 mol-% purity oxygen concentrate is 274 kJ/kg, when a literature value for producing 83 mol-% purity concentrate is

399 kJ/kg. The deviation from literature value can be presumed to be caused by the idealizations made in the modelling of the subprocesses.

Sources of error in the simulation results may include inaccuracy caused by idealization and using estimated initial values in the simulation. The simulation model configuration is described in Chapter 5.1. The modelling of the process devices does not take actual pressure losses, efficiencies and heat losses into consideration, but only an estimated constant value. Also the heat transfer coefficient throughout the heat exchangers is presumed constant. The values used in the model are also given in Chapter 5.1.

Only the process values of streams outside the calculation blocks are known. Hence the process value profiles inside the separation columns can be partly unknown. This causes uncertainty regarding the validity of simulation results, because all of the numerical data the simulation software uses in calculation is not always automatically visible for the user.

The functionality of the Nurmia oxygen enrichment process has previously been researched in studies made at the Institute of Energy and Process Engineering of Tampere University of Technology (Saarenpää 2002; Saarenpää et al. 2004). The main focus of the studies was to confirm the process functionality and furthermore to study its possible applications. However, a simulation model of the process with a possibility to process device dimensioning and design has not previously been made.

The simulation model composed in this thesis is found useful for investigating process properties while altering the process configuration. The results of simulation confirm that the Nurmia oxygen enrichment method is more energy efficient way to produce oxygen concentrate with moderate or high (50-99%) purity than the conventional air separation process Linde-Frankl. The process is also found flexible and several input values of the process can be adjusted in order to alter the product purity or the compression work. Different kinds of heat exchangers, compressors and other process devices can be easily tested by changing the configurations of the simulation blocks until a desired outcome has been reached.

The simulation model however is not able to calculate the development of the process values when the inputs are adjusted. This is because the simulation software is capable of calculating only the equilibrium state of the process and no dynamic calculation is performed.

Different industrial applications using oxygen have different requirements for it. Oxy-combustion for example requires large volume oxygen production (typically over 8000 t/d) with low operating costs and moderate product purity (usually 85-98 mol-%) (Teir et al. 2011; Tranier et al. 2011, p. 968). For this purpose Nurmia oxygen enrichment process seems highly suitable, because it has lower operating costs due to better efficiency and the product purity needed is not as high as for Linde-Frankl process.

# 7. CONCLUSIONS

The Nurmia oxygen enrichment process enables oxygen concentrate production with better efficiency than the current state-of-the-art oxygen separation process Linde-Frankl. The purity of the oxygen product in Nurmia oxygen enrichment process is approximately 50-99 mol-% depending on the process configuration. Lowering the purity decreases the energy consumption. For Linde-Frankl process the oxygen content of the product is 99.5 mol-% or more. The power consumption of compression work for Nurmia process varies from 75 to 111 kWh/t depending on the chosen process configuration, which the simulation model also confirms. For the conventional Linde-Frankl process the power consumption from compression work is approximately 245 kWh/t. The interrelation between the compression works is illustrated in Figure 24.

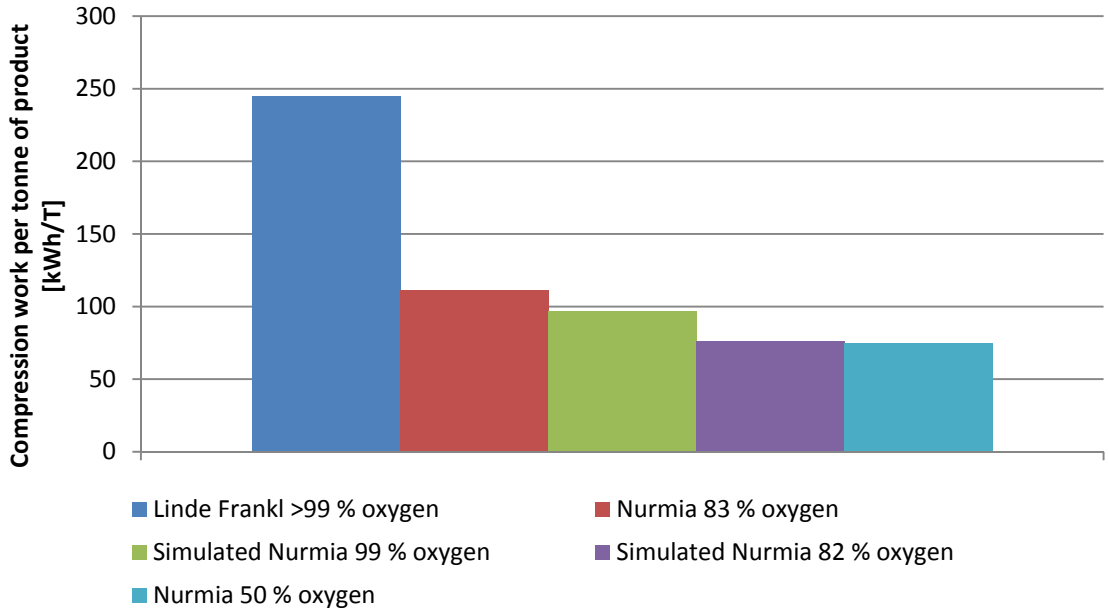


***Figure 24.*** *The power consumption from compression work per tonne oxygen product for Linde-Frankl process manufacturing oxygen product with an oxygen content of over 99 mol-% and Nurmia oxygen enrichment processes manufacturing oxygen products with 50 mol-%, 82 mol-%, 83 mol-% and 99 mol-% oxygen fractions.*

The simulated process manages to generate its own refrigeration, but this requires a heat exchanger surface area of 4.9 $m^2$ for medium purity oxygen product and 7.1 $m^2$ for high purity oxygen product both with a default value of heat transfer coefficient 850 W/(K $m^2$), when the input air flow is 10 kmol/h. Additional refrigeration with a cooling turbine may be more cost effective, if the required heat exchangers are deemed to be more

expensive than the usage of additional refrigeration. This is also affected by the cost of electricity.

The difference between the energy requirements is caused by several reasons. Nurmia process operates at nearly atmospheric and lower than atmospheric pressure, so less energy is needed to compress the air than in Linde-Frankl process that occurs at a higher pressure level. Due to the lower pressure level also the temperature difference between the ends of the two columns is considerately lower for Nurmia process than in Linde-Frankl process. This makes the separation process to be closer to a reversible ideal separation process. The small temperature difference between the columns means that the set-up needs to be thoroughly insulated in order to minimize heat transfer in to the process from the environment. The heat fluxes in the process are easily disturbed by external heat leaks, because the temperature differences within the set-up are small. The lower pressure level in the Nurmia oxygen enrichment process also means that the wall structures do not need to be as strong and robust as in Linde-Frankl process. (Nurmia 2003)

The size and operating time of the air separation plant are important factors to consider when deciding which process option to choose. Also the price of electricity is an important factor. Increasing the size of heat exchange surface decreases the compressor power needed. Furthermore, increasing heat exchanger surface increases the plant investment costs and increasing the compressor power increases the operating costs. The operation practice of the plant and the purity requirement of the product determine which configuration is the best suited and the most economical for the plant in question.

This simulation model is found useful for investigating process parameters, such as the need of compression power, possible additional refrigeration, internal heat streams and process yield with chosen input parameters. A sensitivity analysis is carried out in order to investigate the effects of varying some of the process variables and to verify the functionality of the simulation model. The pressure in the first stage of the low pressure column is varied and the effects are investigated. A lowered pressure level such as 0.2 bar is found to increase the compressor work needed to compress the oxygen product and decrease the work needed for nitrogen concentrate compression. This is because the mass volumes of the oxygen and nitrogen streams change in the opposite direction when the pressure of the first stage of the low pressure column is lowered. Lowering the first stage pressure level in low pressure column also increases the oxygen content of the process product, because the enriching factor of oxygen in nitrogen-oxygen mixtures is higher at lower pressure levels.

A model of the basic version of Nurmia process is created with a possibility for sensitivity analysis. With the model process parameters, required external energy, internal heat streams and process yield with chosen input parameters are studied.

Aspen Plus is found to be a practical tool for the optimization and control of the Nurmia oxygen enrichment process. A drawback to the software is that the version used in the simulation does not perform dynamic calculations but only steady-state. The more complex the process, the harder it is to make the simulation converge, because the calculation requires increasingly accurate initial values and the number of unknown variables in the calculation becomes too large to be solved.

The simulation model is a more ideal process than a real one. In a real process the efficiency of the process would increase if the production volume was increased. The relative heat losses decrease when the production volume increases. This is because the total losses do not grow as much as the process energy consumption when the production volume is increased. Hence the fraction of losses from the total energy requirement decreases.

Other available process options should also be investigated. These include reflux streams to achieve higher purity of product and yield to feed ratio. The optimization of the heat exchanger arrangement should be done on the grounds of exergy in order to achieve the most efficient process.

The simulation model illustrates an equilibrium state of the process. Only the equilibrium model is studied, but a dynamic simulation of the process is also needed for further studies in order to investigate the functionality of the process start-up and process control. A demo-scale Nurmia oxygen enrichment plant should be built to verify the simulation results and the functionality of the different process configurations proposed in this work.

# REFERENCES

R. Agrawal & D. M. Herron. AIR LIQUEFACTION: DISTILLATION, In Encyclopedia of Separation Science, edited by I. D. Wilson, E. R. Adlard, M Cooke & C. F. Poole. Academic Press, Oxford, 2000, pp. 1895-1910.

Aspen Plus, version 8.6. Aspen Technology Inc. Bedford, Massachusetts, USA 2014.

Y. S. Bang, J. H. Chun, B. D. Chung & G. C. Park. (2009). Improvements of Condensation Heat Transfer Models in MARS Code for Laminar Flow in Presence of Non-Condensable Gas. Nuclear Engineering and Technology. Vol. 41(8), pp. 1015-1024.

Y. Bayazitoglu & M. N. Özisik, Elements of Heat Transfer. McGraw-Hill. 1988. International Edition. 602 p.

G. T. Brower & G. Thodos. (1968). Vapor Pressures of Liquid Oxygen Between the Triple Point and Critical Point. Journal of Chemical & Engineering Data. Vol. 13(2), pp. 262-264.

W. F. Castle. (2002). Air Separation and Liquefaction: Recent Developments and Prospects for the Beginning of the New Millennium. International Journal of Refrigeration. Vol. 25, pp. 158-172.

P. J. Chenier, Survey of Industrial Chemistry. 3rd edition. Springer US. 2002. 513 p.

A. P. Colburn & O. A. Hougen. (1934). Design of Cooler Condensers for Mixtures of Vapors with Noncondensing Gases. Industrial & Engineering Chemistry. Vol. 26(11), pp. 1178-1182.

R. L. Cornelissen & G. G. Hirs. (1997) Exergetic Optimization of a Heat Exchanger. Energy Conversion and Management. Vol. 38(15), pp. 1567-1576.

A. Darde, R. Prabhakar, J. P. Tranier & N. Perrin. (2009). Air Separation and Flue Gas Compression and Purification Units for Oxy-Coal Combustion Systems. Energy Procedia. Vol. 1(1), pp. 527-534.

A. Faghri & Y. Zhang. Transport Phenomena in Multiphase Systems. Academic Press. 2006, 1030 p.

C. Fu & T. Gundersen. (2012). Using Exergy Analysis to Reduce Power Consumption in Air Separation Units for Oxy-Combustion Processes. Energy Vol. 44(1), pp. 60-68.

T. M. Flynn. Cryogenic Engineering. Taylor & Francis. 2004. 2nd edition, 912 p.

J. M. Kay & R. M. Nedderman, Fluid Mechanics and Transfer Processes. Cambridge University Press. 1985. 602 p.

N. I. Kolev, Multiphase Flow Dynamics 3 - Thermal Interactions. Springer. 2011. 4th edition, Berlin, Germany. 683 p.

A. Laesecke, R. Krauss, K. Stephan & W. Wagner. (1990). Transport Properties of Fluid Oxygen. Journal of Physical and Chemical Reference Data, Vol. 19(5), pp. 1089-1122 in Thermophysical Properties of Fluid Systems in NIST Chemistry WebBook, NIST Standard Reference Database Number 69. Editors. P. J. Linstrom & W. G. Mallard. National Institute of Standards and Technology. Gaithersburg MD.
http://webbook.nist.gov, (accessed on 25.4.2015).

E.W. Lemmon, M. O. McLinden & D.G. Friend. Thermophysical Properties of Fluid Systems in NIST Chemistry WebBook, NIST Standard Reference Database Number 69. National Institute of Standards and Technology. Gaithersburg MD.
http://webbook.nist.gov, (accessed on 17.8.2015).

Linde Engineering. (2009). Cryogenic Air Separation – History and Technological Progress. Company booklet, The Linde Group.

J. J. McKetta. Heat Transfer Design Methods. Marcel Dekker, inc. 1992. 615 p.

A. Mersmann, M. Kind & J. Stichlmair. Thermal Separation Technology - Principles, Methods, Process Design. Springer-Verlag Berlin Heidelberg. 2011. 675 p.

A. F. Mills. Basic Heat and Mass Transfer. Prentice Hall. 1999. 2nd edition, New Jersey, USA. 1000 p.

M. Nurmia, (2003). Finnish patent 111187, Normaalipaineessa toimiva prosessi hapen tai hapella rikastetun ilman tuottamiseksi, granted: 13.06.2003.

Oxyfuel Combustion Conference 3. Conference Summary. IEA Greenhouse Gas R&D Programme. 3rd Oxyfuel Combustion Conference. Ponferrada, Spain. 9th – 13th September 2013. 14 p.

C. Panzarella & M. Kassemi. (2009). One-Dimensional Model of Evaporation and Condensation in the Presence of a Noncondensable Gas with Applications to Cryogenic Fluid Storage. International Journal of Heat and Mass Transfer. Vol. 52, pp. 3767–3777.

D.-Y. Peng & D. B. Robinson. (1976) A New Two-Constant Equation of State. Industrial & Engineering Chemistry Fundamentals. Vol. 15(1), pp.59–64.

R. Raiko. (2013). KEB-43200 Voimalaitostekniikka. Lecture notes 2013. Tampere University of Technology. 248 p.

R. Raiko & I. Saarenpää. (2014). KEB-43100 Höyrytekniikka. Lecture notes 2014. Tampere University of Technology. 254 p.

I. Saarenpää, (2002). Uuden hapenrikastusprosessin kehittäminen. Tampere University of Technology. Institute of Energy and Process Engineering.

I. Saarenpää, H. Knuutila & P. Haukka, (2004). Cryogenic Method Operating at Normal Pressure and Below for Enriching the Oxygen Content in Air. 21st Annual International Pittsburgh Coal Conference, 13-17 September 2004. Osaka, Japan. 21 p.

R. Schmidt & W. Wagner. (1985). A New Form of the Equation of State for Pure Substances and its Application to Oxygen, Fluid Phase Equilibria, Vol. 19(3), pp. 175-200 in Thermophysical Properties of Fluid Systems in NIST Chemistry WebBook, NIST Standard Reference Database Number 69. National Institute of Standards and Technology. Gaithersburg MD. http://webbook.nist.gov, (accessed on 25.4.2015).

A. Shavit & C. Gutfinger, Thermodynamics: From Concepts to Applications. CRC Press, Taylor & Francis Group. 2009. 2nd edition. 649 p.

R. Smith & M. Jobson. DISTILLATION, In Encyclopedia of Separation Science. Edited by I. D. Wilson, E. R. Adlard, M. Cooke & C. F. Poole. Academic Press, Oxford, 2000. pp. 84-103.

R. Span, E.W. Lemmon, R. T. Jacobsen, W. Wagner & A. Yokozeki. (2000). A Reference Equation of State for the Thermodynamic Properties of Nitrogen for Temperatures from 63.151 to 1000 K and Pressures to 2200 MPa, Journal of Physical and Chemical Reference Data Vol. 29(6), pp. 1361-1433 in Thermophysical Properties of Fluid Systems in NIST Chemistry WebBook, NIST Standard Reference Database Number 69. National Institute of Standards and Technology. Gaithersburg MD.
http://webbook.nist.gov, (accessed on 25.4.2015).

H. Struchtrup, Thermodynamics and Energy Conversion. Springer eBooks. Springer Berlin Heidelberg. 2014. 597 p.

S. Teir, T. Pikkarainen, L. Kujanpää, E. Tsupari, J. Kärki, A. Arasto & S. Aatos. (2011). Hiilidioksidin talteenotto ja varastointi (CCS). Teknologiakatsaus. VTT Working papers 161. VTT. 103 p.

K.D. Timmerhaus & R. Reed. Cryogenic Engineering: Fifty Years of Progress. Springer Science & Business Media, 2007. 374 p.

J. P. Tranier, R. Dubettier, A. Darde, & N. Perrin. (2011). Air Separation, Flue Gas Compression and Purification Units for Oxy-Coal Combustion Systems. Energy Procedia. Vol. 4. pp. 966–971.

G. A. Zimmerli, M. Asipauskas, N.T. Van Dresar. (2010). Empirical Correlations for The Solubility of Pressurant Gases in Cryogenic Propellants, Cryogenics, Vol. 50(9), pp. 556-560.